The GEOFLOW-Experiment as a Spherical Bifurcation Problem

Diploma Thesis

presented by

Alexander Lohse

at the Department of Mathematics of the University of Hamburg

1. Examiner: Prof. Dr. Reiner Lauterbach
2. Examiner: Prof. Dr. Ingenuin Gasser

Hamburg, July 2010

The eyes of the LORD search the whole Earth in order to strengthen those whose hearts are fully committed to him.

2 Chronicles 16:9

Contents

1 Introduction

In this thesis we investigate the spherical Bénard problem from an analytical viewpoint. There is an abundance of literature concerning this topic, dating back over the last decades. The main objective of this work is to introduce mathematical concepts that are crucial for a bifurcation analysis of the governing equations and sum up the results that have been obtained by other authors before. Moreover, we discuss the geophysical background of the problem and the GEOFLOW-experiments, a recent research initiative by a team of scientists at the BTU Cottbus.

In the classical spherical Bénard problem an incompressible fluid is confined between two concentric spherical shells with the inner shell being uniformly heated. Furthermore, a radially symmetric gravity field is imposed on the domain. This leads to a system of partial differential equations that are invariant under the natural action of the orthogonal group $O(3)$. The task is then to study the evolving flow patterns which of course depend on a number of parameters and quantities, such as the viscosity and thermal conductivity of the fluid, the temperature gradient and the ratio η of the radii of the spheres.
For a small temperature difference between the inner and outer boundary we observe pure heat conduction without actual movement of the fluid as the stable solution to the governing equations. However, once the difference exceeds a critical value convection sets in, i.e., the heated fluid rises up from the inside and cools off near the outer boundary before it sinks downwards again. This qualitative change in behavior corresponds to a (steady-state) bifurcation in the governing equations. In this context we consider the Rayleigh number as the bifurcation parameter and denote it by C_ℓ in accordance with [Chandrasekhar (1961)]. It is a non-dimensional number that is proportional to the temperature difference between the boundaries and inversely proportional to the kinematic viscosity of the fluid, see section 3.3 for a rigorous definition. In this way determining the critical temperature difference for the onset of convection becomes equivalent to determining a critical Rayleigh number C_ℓ.

The present thesis is divided into the following parts: In Chapter 2 we outline the mathematical concepts that we apply to the Bénard problem later. This includes elementary results of equivariant theory, spherical harmonics and center manifold reduction.
The actual analysis of the Bénard problem is done in Chapter 3: We prove that the bifurcation is of steady-state type and exploiting the spherical geometry of the domain we discover the form of the critical eigenspaces. Generically a single subspace V_ℓ, consisting of spherical harmonics of degree ℓ, goes unstable to cause the onset of convection. As the next step we

regard η, the radius ratio of the spheres, as a secondary bifurcation parameter. It follows then that for certain values η_0 the two spaces V_ℓ and $V_{\ell+1}$ lose their stability simultaneously. This phenomenon is called mode interaction and exhibits particularly interesting dynamics. A center manifold reduction enables us to reduce the (infinite-dimensional) system of equations to eight dimensions for the simplest case of mode interaction in which we investigate the presence of heteroclinic cycles.
Finally Chapter 4 is concerned with the geophysical motivation for the study of the Bénard problem. It derives primarily from the discovery of convection in the interior of the Earth, particularly in the mantle and in the outer core. We also give an overview of the GEOFLOW project, a recent research initiative by the *Chair of Aerodynamics and Fluid Mechanics* of the BTU in Cottbus where experiments have been performed in the microgravity environment of the International Space Station (ISS).

Acknowledgments

First and foremost I would like to thank Professor Lauterbach for introducing me to this interesting area of research. He left me all the freedom I could wish for in choosing the exact contents of my thesis while at the same time being available to answer my questions or give helpful hints whenever needed. I am also grateful for the pleasant working atmosphere among my fellow students who provided helpful mathematical advice, a constantly cheerful attitude and countless cups of coffee. I would like to express my gratitude towards Christoph Egbers, Philippe Beltrame and Mary Fowler for responding to my emails and answering my questions, sending me research papers I asked them for and allowing me to reproduce some of their figures in my work.
My parents supported and encouraged me tremendously throughout my studies and helped me complete my thesis by proofreading carefully. The latter also goes for my friend Phil. Last but certainly not least I thank my wonderful wife Jojo for supporting me in every possible way by simply being herself – I love you to bits!

2 Mathematical Basics

2.1 The Equivariant Branching Lemma

In this section we introduce some basic features of systems of differential equations with symmetry. Our main objective is to prove the equivariant branching lemma, an elementary but powerful result in the theory of systems with symmetry which will later enable us to simplify the analysis of the Bénard problem.
The theory in this section is restricted to $\mathbb{R}^n$ because that is enough for our later purposes. First of all we need to formalize what we mean when we say that a system of equations obeys a certain symmetry. To this end we recall some fundamental definitions and techniques of group actions and representation theory. Throughout this chapter we take Γ to be a compact Lie group, even if we do not say so explicitly every time. We generally proceed along the lines of [Golubitsky and Stewart (2002)], Chapter 1, except for the remark prior to Theorem 11 which can be found in [Golubitsky et al. (1988)].

Definition 1. Let Γ be a (not necessarily compact) Lie group and V a vector space. A **(left) action** of Γ on V is a map $\rho : \Gamma \times V \to V$ satisfying the following properties:

- $\rho(e,v) = v \quad \forall v \in V$, e being the neutral element in Γ
- $\rho(\gamma_1\gamma_2,v) = \rho(\gamma_1,\rho(\gamma_2,v)) \quad \forall v \in V,\ \forall \gamma_1,\gamma_2 \in \Gamma$

A **right action** is defined analogously. Throughout this work we refer to left actions simply as **actions** unless explicitly stated otherwise. To simplify notation we write $\gamma \cdot v$ or simply γv instead of $\rho(\gamma,v)$.

It is well known that an action can also be viewed as a homomorphism

$$\Gamma \to GL(V),\ \gamma \mapsto (v \mapsto \gamma v).$$

Such a homomorphism is also commonly referred to as a **representation of** Γ **on** V. We are now able to formalize the meaning of symmetry of a dynamical system in terms of group actions in the following definition.

Definition 2. Let $\dot{x} = f(x,\lambda)$ be a parameter-dependent system of ordinary differential equations defined on $\mathbb{R}^n$, $\lambda \in \mathbb{R}$ and $f \in C^\infty(\mathbb{R}^n \times \mathbb{R}, \mathbb{R}^n)$. Let a compact Lie group Γ act on $\mathbb{R}^n$. We call $\gamma \in \Gamma$ a **symmetry** of the system if for every solution $x(t)$ the curve $\gamma x(t)$ is also a solution.

Consider now a system $\dot{x} = f(x, \lambda)$ and a symmetry $\gamma \in \Gamma$ as defined above. For now let us neglect the parameter λ in our notation since it does not influence the following considerations. Later, however, we turn our attention to bifurcations and the role of λ becomes crucial. Let $x(t)$ be a solution to the system and set $y(t) := \gamma x(t)$. The following calculation leads to the next definition:

$$\dot{y}(t) = \gamma \dot{x}(t) = \gamma f(x(t))$$

and also

$$\dot{y}(t) = f(y(t)) = f(\gamma x(t))$$

so therefore for all t for which the solution exists we have

$$\gamma f(x(t)) = f(\gamma x(t)).$$

If a solution exists for arbitrary initial conditions this is equivalent to $f(\gamma x) = \gamma f(x)$ for all $x \in \mathbb{R}^n$.

Definition 3. Let Γ act on $\mathbb{R}^n$ and let $f : \mathbb{R}^n \to \mathbb{R}^n$. We call f **Γ-equivariant** if $f(\gamma x) = \gamma f(x)$ for all $x \in \mathbb{R}^n$ and $\gamma \in \Gamma$. Alternatively we say that f **commutes with** Γ.

Another important concept is that of symmetry of a solution to a system of equations. Consider an equilibrium $x_0 \in \mathbb{R}^n$, i.e., $f(x_0) = 0$. We say that $\delta \in \Gamma$ is a symmetry of x_0 if $\delta x_0 = x_0$. The set of $\delta \in \Gamma$ with this property forms a subgroup of Γ. In fact, we can define this subgroup for any $x \in \mathbb{R}^n$, not just for equilibria:

Definition 4. For $x \in \mathbb{R}^n$ we call $\Sigma_x = \{\gamma \in \Gamma \mid \gamma x = x\}$ the **isotropy subgroup** of x.

Note that a symmetry of the system is not necessarily a symmetry of each of its solutions. Recalling that the **group orbit** of $x \in \mathbb{R}^n$ is the set $\{\gamma x \mid \gamma \in \Gamma\}$ we find that for $\gamma \in \Gamma$ the isotropy subgroups of x and γx are conjugates, in fact $\Sigma_{\gamma x} = \gamma \Sigma_x \gamma^{-1}$. So isotropy subgroups along group orbits are conjugates of one another.
For many purposes it proves useful to treat conjugate equilibria (or conjugate solutions in general) as one, which prompts us to consider conjugacy classes of isotropy subgroups. An obvious relation between subgroups is that of containment and it is naturally carried over to the conjugacy classes. The partially ordered set (by inclusion) of conjugacy classes of isotropy subgroups is commonly called the **isotropy lattice** and in some situations maximal subgroups (in terms of containment) are of special interest.

Instead of determining the symmetries of a known solution one can turn things around and ask the following question: For a given subgroup Σ of Γ is there a solution with the elements of Σ as its symmetries? Via this approach we systematically search for solutions of a given system that are subject to symmetries given by an isotropy subgroup.

Definition 5. Let $\Sigma \subset \Gamma$ be a subgroup. Then we define the **fixed-point space** of Σ to be

$$\text{Fix}(\Sigma) = \{x \in \mathbb{R}^n \mid \sigma x = x \quad \forall \sigma \in \Sigma\}.$$

Definition 6. An isotropy subgroup Σ of Γ is called **axial** if $\dim(\text{Fix}(\Sigma)) = 1$.

Proposition 7. *Let $f : \mathbb{R}^n \to \mathbb{R}^n$ be Γ-equivariant and $\Sigma \subset \Gamma$ a subgroup of Γ. Then*

$$f(\text{Fix}(\Sigma)) \subset \text{Fix}(\Sigma).$$

Proof. Let $\sigma \in \Sigma$ and $x \in \text{Fix}(\Sigma)$. Then $\sigma f(x) = f(\sigma x) = f(x)$ and therefore $f(x) \in \text{Fix}(\Sigma)$. □

Recalling $\Sigma_{\gamma x} = \gamma \Sigma_x \gamma^{-1}$ from above we find $\text{Fix}(\gamma \Sigma_x \gamma^{-1}) = \text{Fix}(\Sigma_{\gamma x}) = \gamma \text{Fix}(\Sigma_x)$ which yields the next result.

Proposition 8. *Let $x(t)$ be a solution of a Γ-equivariant system $\dot{x} = f(x)$. Then $\Sigma_{x(0)} = \Sigma_{x(t)}$ for all $t \in \mathbb{R}$, i.e., along a solution trajectory we always have the same isotropy subgroup.*

Proof. $\text{Fix}(\Sigma_{x(0)})$ is flow-invariant by the previous proposition, so we have $x(t) \in \text{Fix}(\Sigma_{x(0)})$ for all t. That means $\Sigma_{x(0)} \subset \Sigma_{x(t)}$. Now the trajectory through $x(t)$ also runs through $x(0)$, so by the same argument $\Sigma_{x(t)} \subset \Sigma_{x(0)}$ and thus $\Sigma_{x(0)} = \Sigma_{x(t)}$. □

These propositions show us that when looking for solutions with symmetry group $\Sigma \subset \Gamma$ we can restrict our search to the space $\text{Fix}(\Sigma)$ which is usually a space of lower dimension than $\mathbb{R}^n$. Therefore this can mean a significant simplification of the original problem. Following this line of reasoning it should be particularly easy to find solutions with symmetry Σ when Σ is a maximal subgroup in terms of the partial ordering of the isotropy lattice as in that case $\dim(\text{Fix}(\Sigma))$ is smallest. Before we go about justifying this assumption we need a few more elementary concepts.

Definition 9. A subspace $V \subset \mathbb{R}^n$ is called **Γ-invariant** if $\gamma v \in V$ for all $v \in V, \gamma \in \Gamma$.

Note that $\mathbb{R}^n$, $\{0\}$ and $\text{Fix}(\Gamma)$ are always Γ-invariant.

Definition 10. We call a subspace $W \subset \mathbb{R}^n$ **Γ-irreducible** if W and $\{0\}$ are its only Γ-invariant subspaces. Equivalently we say that Γ **acts irreducibly** on W or that we have an **irreducible representation** of Γ on W.

In order to state and prove the next theorem it comes in handy to know that every compact Lie group Γ that acts on $\mathbb{R}^n$ can be identified with a subgroup of the orthogonal group $O(n)$. In other words, there exists an inner product such that for every $\gamma \in \Gamma$ the associated matrix $\rho_\gamma = \rho(\gamma, \cdot)$ is orthogonal. This product is then Γ-invariant. The proof of this is sketched in [Golubitsky et al. (1988)], Chapter XII, §1(c). We use the existence of an invariant inner product to prove the next theorem.

Theorem 11. *Let $\Gamma \subset O(n)$ be a compact Lie group. Then there exist Γ-irreducible subspaces V_1,...V_k such that*

$$\mathbb{R}^n = V_1 \oplus ... \oplus V_k$$

Proof. Assume that Γ does not act irreducibly on $\mathbb{R}^n$. Then there is an invariant subspace W that is neither $\mathbb{R}^n$ nor $\{0\}$. Consider now $W^\perp = \{x \in \mathbb{R}^n \mid \langle x,y\rangle = 0 \quad \forall y \in W\}$ where $\langle \cdot\,,\, \cdot \rangle$ is the aforementioned Γ-invariant inner product. To see that $W^\perp$ is also a Γ-invariant subspace let $y \in W^\perp$ and calculate for any $w \in W$

$$\langle \gamma y,w\rangle = \langle y,\gamma^{-1}w\rangle = \langle y,\tilde{w}\rangle = 0$$

where the last equality holds since $\tilde{w} \in W$ because of the Γ-invariance of W. Thus we have the decomposition $\mathbb{R}^n = W \oplus W^\perp$ into Γ-invariant subspaces. Since $\mathbb{R}^n$ is finite-dimensional we can repeat this process until Γ acts irreducibly on all elements of the decomposition. □

For the equivariant branching lemma we need to impose an even stronger condition on the action of Γ, namely that of absolute irreducibility. To motivate the next definition we reintroduce the parameter λ into our equations, consider a Γ-equivariant mapping f and differentiate both sides of the equality $f(x,\lambda)\gamma = f(\gamma x,\lambda)$ using the chain rule to obtain

$$\mathrm{D}f_{(\gamma x,\lambda)}\gamma = \gamma \mathrm{D}f_{(x,\lambda)}$$

so for $x = 0$

$$\mathrm{D}f_{(0,\lambda)}\gamma = \gamma \mathrm{D}f_{(0,\lambda)}.$$

This means that the linear map $\mathrm{D}f_{(0,\lambda)}$ commutes with Γ. If now the action of Γ itself already imposes certain conditions on the commuting linear maps we can a priori deduce something about the differential of our equivariant mapping at $(0,\lambda)$. That is why the following definition proves useful.

Definition 12. We call the action (or again the representation) of Γ on $\mathbb{R}^n$ **absolutely irreducible** if the only linear maps that commute with Γ are multiples of the identity, i.e., they are of the form $c\mathbb{1}$, $c \in \mathbb{R}$.

In the setting described above this means as soon as we know that the action is absolutely irreducible it is clear that the differential of f is of the form $\mathrm{D}f_{(0,\lambda)} = c(\lambda)\mathbb{1}$. Of course it is now natural to ask whether or not we can reasonably expect the action of Γ to be absolutely irreducible generically. The answer to this question is given by the next theorem.

Theorem 13. *Consider an ordinary differential equation $\dot{x} = f(x,\lambda)$ where f is Γ-equivariant and suppose there is a branch of Γ-invariant equilibria $x_0(\lambda)$. Moreover, let there be a steady-state bifurcation for some parameter value λ_0 which implies that the Jacobian matrix $A_0 := \mathrm{D}f_{(x_0(\lambda_0),\lambda_0)}$ is singular. Then generically the following is true:*

(a) The only eigenvalue of A on the imaginary axis is 0.
(b) The generalized eigenspace belonging to 0 *is* $\ker A_0$.
(c) Γ *acts absolutely irreducible on* $\ker A_0$.

This theorem underlines the importance of absolute irreducibility in the theory of steady-state bifurcations as the group action on the kernel of the linearization is generically absolutely irreducible. We are now able to state the central theorem of this section.

Lemma 14 (Equivariant Branching Lemma)**.** *Let* Γ *be a compact Lie group that acts absolutely irreducibly on* $\mathbb{R}^n$ *and let* $\Sigma \subset \Gamma$ *be an axial subgroup. Consider an equivariant mapping*

$$f : \mathbb{R}^n \times \mathbb{R} \to \mathbb{R}^n,$$

i.e., $f(0,\lambda) \equiv 0$ *and* $\mathrm{D}f_{(0,\lambda)} = c(\lambda)\mathbb{1}$. *Moreover, assume that*

(a) $c(0) = 0$
(b) $c'(0) \neq 0$.

Then there exists a unique branch of solutions to $f(x,\lambda) = 0$ *emanating from* $(0,0)$ *where the symmetry of the solutions is* Σ.

Note that (a) is the condition that is necessary for a bifurcation to occur. Condition (b) is commonly called the "eigenvalue crossing condition". This result means that generically in a Γ-symmetric bifurcation problem there exists a solution branch for every isotropy subgroup with one-dimensional fixed-point space.

Proof. Let $0 \neq v \in \mathrm{Fix}(\Sigma)$. Then $\mathrm{Fix}(\Sigma) = \mathrm{span}_{\mathbb{R}}\{v\}$ since $\dim(\mathrm{Fix}(\Sigma)) = 1$. Because of Proposition 7 this means that there is a function $h : \mathbb{R} \times \mathbb{R} \to \mathbb{R}$ such that

$$f(tv,\lambda) = h(t,\lambda)v$$

and of course $h(0,\lambda) = f(0,\lambda) = 0$. Considering the Taylor series of h we find that $h(t,\lambda) = tk(t,\lambda)$ with a function k that satisfies $k(0,0) = c(0) = 0$ and $k_\lambda(0,0) = c'(0) \neq 0$ since (a) and (b) hold. Therefore we can apply the implicit function theorem and obtain a unique $\lambda(t)$ such that $\lambda(0) = 0$ and $k(t,\lambda(t)) \equiv 0$. Consequently,

$$f(tv,\lambda(t)) = h(t,\lambda(t))v = tk(t,\lambda(t))v = 0$$

which means that for every $\lambda(t)$ we have an equilibrium tv. By construction we have $tv \in \mathrm{Fix}(\Sigma)$ and thus there exists a (local) branch of solutions with symmetry group Σ. □

2.2 Invariant Theory

After studying Γ-equivariant (linear) maps in the context of absolute irreducibility in the previous section we now want to present an efficient way of describing general (nonlinear) mappings that commute with a group action. This can be of interest when trying to determine the Taylor series expansion of the right hand side of a reduced system of differential equations, e.g. after a center manifold reduction has been performed, see section 2.4. Two important theorems form the center of this section, they enable us to characterize Γ-invariant polynomials and Γ-equivariant polynomials mappings. Both theorems can be found in [Golubitsky et al. (1988)], Chapter XII, §4 and §5, respectively, for the proofs see §6.

A scalar function $\varphi : V \to \mathbb{R}$ is called Γ-invariant if we have

$$\varphi(\gamma x) = \varphi(x) \tag{2.1}$$

for all $\gamma \in \Gamma$ and $x \in V$. For φ to be Γ-invariant it obviously suffices to show that (2.1) holds for a set of generators of the group Γ.
Let us denote the set of Γ-invariant polynomials by $\mathcal{P}(\Gamma)$. It bears the algebraic structure of a ring since sums and products of Γ-invariant polynomials are also Γ-invariant. The Hilbert-Weyl theorem makes an important assertion about this ring, namely that it is generated by a finite set of elements:

Theorem 15 (Hilbert-Weyl Theorem)**.** *Let a compact Lie group Γ act on a vector space V. Then there exists a finite Hilbert basis for the ring of Γ-invariant polynomials $\mathcal{P}(\Gamma)$.*

By **Hilbert basis** we mean a set of Γ-invariant polynomials such that every invariant polynomial can be written as a polynomial function of the elements of our basis. The actual computation of such a basis, which by no means has to be unique, can be quite complicated and often requires a few tricks, but let us consider a simple example:

Let the group $\mathbb{Z}_2 = \{\pm 1\}$ act on $\mathbb{R}$ by $-1 \cdot x = -x$. Then for a function $\varphi : \mathbb{R} \to \mathbb{R}$ to be $\mathbb{Z}_2$-invariant we need

$$\varphi(-1 \cdot x) = \varphi(-x) \stackrel{!}{=} \varphi(x)$$

to hold. Therefore, the invariant functions are just the even functions which in turn means that if p is a $\mathbb{Z}_2$-invariant polynomial we find another polynomial q such that $p(x) = q(x^2)$. Thus in this case the Hilbert basis of $\mathcal{P}(\mathbb{Z}_2)$ is simply $\{x^2\}$, because every invariant polynomial can be written as a polynomial in x^2. Now let us turn our attention to equivariant mappings by starting with an elementary observation:

Proposition 16. *If $f : V \to V$ is a Γ-equivariant mapping and φ a Γ-invariant function, then the product φf is again Γ-equivariant.*

Proof. We simply calculate

$$\begin{aligned}(\varphi f)(\gamma x) &= \varphi(\gamma x) f(\gamma x) \\ &= \varphi(x)\gamma f(x) \\ &= \gamma\varphi(x) f(x) \\ &= \gamma[\varphi f(x)].\end{aligned}$$

□

Definition 17. We denote by $\vec{\mathcal{P}}(\Gamma)$ the space of Γ-equivariant polynomial mappings $V \to V$.

It follows from proposition 16 that $\vec{\mathcal{P}}(\Gamma)$ is a module over the ring $\mathcal{P}(\Gamma)$ of Γ-invariant polynomials.

Theorem 18. *Let a compact Lie group Γ act on a vector space V. Then there exists a finite set of Γ-equivariant polynomials that generate the module $\vec{\mathcal{P}}(\Gamma)$.*

If we extend the example from above we find that in this case the $\mathbb{Z}_2$-equivariant mappings are all odd mappings $f : \mathbb{R} \to \mathbb{R}$ since

$$f(-1 \cdot x) = f(-x) \stackrel{!}{=} -f(x)$$

has to hold. As a matter of fact every such mapping can be written as the product of an even function with x. This can be seen in the following way: Since $f(0) = 0$ Taylor's theorem enables us to write $f(x) = h(x)x$. Now f is odd, so

$$h(x)x = f(x) = -f(-x) = h(-x)x$$

which means that h is even. By the previous remarks we know that we can write $h(x) = k(x^2)$, so we have $f(x) = k(x^2)x$. Therefore in this case $\vec{\mathcal{P}}(\mathbb{Z}_2)$ is generated by a single $\mathbb{Z}_2$-equivariant polynomial, namely x.

Of course the example considered here was very simple to calculate. In section 3.4 we face a similar task in a significantly more difficult setting but still this should suffice as an indication of the methods that exist to classify the possible equivariant right hand sides for a system with symmetry.

2.3 Spherical Harmonics

The spherical harmonics $Y_{\ell m}$ are scalar functions that form an orthonormal basis of the Hilbert space $L^2(S^2)$ and therefore any function in this space can be expanded in spherical harmonics. In this section we derive these functions from Laplace's equation and introduce some of their basic properties. These concepts are crucial for the understanding of mode interaction in the spherical Bénard problem. The steps that we omit in our discussion, in particular the arguments that are due to properties of the associated Legendre functions, can be found in [Duff and Naylor (1966)], Chapter 9.

Derivation and Properties

Consider a scalar function f defined on the three-dimensional unit ball $B_1(0)$ and Laplace's equation

$$0 = \Delta f(r,\vartheta,\varphi)$$

with Δ written in spherical coordinates:

$$\Delta = \frac{\partial^2}{\partial r^2} + \frac{2}{r}\frac{\partial}{\partial r} + \frac{1}{r^2}\left(\frac{\partial^2}{\partial \vartheta^2} + \frac{\cos\vartheta}{\sin\vartheta}\frac{\partial}{\partial\vartheta} + \frac{1}{\sin^2\vartheta}\frac{\partial^2}{\partial\varphi^2}\right) =: \Delta_r + \frac{1}{r^2}\Delta_{\vartheta,\varphi}$$

The spherical harmonics $Y_{\ell m} \in L^2(S^2)$ are obtained as solutions of the angular part $\Delta_{\vartheta,\varphi}$ of this equation, i.e., the expression written in brackets above. In order to solve the equation we separate the variables in the following way:

$$f(r,\vartheta,\varphi) = R_\ell(r)Y_{\ell m}(\vartheta,\varphi)$$

A short calculation yields

$$0 \stackrel{!}{=} \Delta(R_l Y_{\ell m}) = (\Delta_r + \frac{1}{r^2}\Delta_{\vartheta,\varphi})(R_l Y_{\ell m}) = Y_{\ell m}\cdot\Delta_r R_\ell + \frac{1}{r^2}R_\ell\cdot\Delta_{\vartheta,\varphi}Y_{\ell m}$$

and thus

$$\frac{r^2\Delta_r R_\ell}{R_\ell} = -\frac{\Delta_{\vartheta,\varphi}Y_{\ell m}}{Y_{\ell m}} = \text{const}$$

where the constant is chosen to be $\ell(\ell+1)$ which proves useful later on. Therefore we obtain the following partial differential equation for the angular part:

$$\Delta_{\vartheta,\varphi}Y_{\ell m} = -\ell(\ell+1)Y_{\ell m}$$

This is solved by another separation of variables of the form $Y_{\ell m}(\vartheta,\varphi) = \Theta_{lm}(\vartheta)\cdot\Phi_m(\varphi)$ which leads to

$$\frac{\sin^2\vartheta}{\Theta_{lm}(\vartheta)}\left(\frac{\mathrm{d}^2}{\mathrm{d}\vartheta^2} + \frac{\cos\vartheta}{\sin\vartheta}\frac{\mathrm{d}}{\mathrm{d}\vartheta}\right)\Theta_{lm}(\vartheta) + \sin^2(\vartheta)\ell(\ell+1) = -\frac{1}{\Phi_m(\varphi)}\frac{\mathrm{d}^2}{\mathrm{d}\varphi^2}\Phi_m(\varphi) = \text{const}$$

where this time m^2 is a suitable choice for the constant. That leaves us with two ordinary differential equations. The equation for $\Phi_m(\varphi)$,

$$\frac{\mathrm{d}^2}{\mathrm{d}\varphi^2}\Phi_m(\varphi) = -m^2\Phi_m(\varphi),$$

is solved by $\Phi_m(\varphi) = A\mathrm{e}^{\mathrm{i}m\varphi}$ with $A \in \mathbb{R}$ as one can easily see. The periodicity condition $\Phi_m(\varphi+2\pi) = \Phi_m(\varphi)$ of the sphere restricts the values of m to integers and by normalizing Φ_m as an L^2-function through

$$1 \stackrel{!}{=} \|\Phi_m\|_{L^2} = \langle\Phi_m,\overline{\Phi_m}\rangle = \int_{-\pi}^{\pi}\Phi_m(\varphi)\overline{\Phi_m(\varphi)}\,\mathrm{d}\varphi = \int_{-\pi}^{\pi}A^2\mathrm{e}^{\mathrm{i}m\varphi}\mathrm{e}^{-\mathrm{i}m\varphi}\,\mathrm{d}\varphi = 2\pi A^2$$

we obtain $A = \frac{1}{\sqrt{2\pi}}$ and thus $\Phi_m(\varphi) = \frac{1}{\sqrt{2\pi}}\mathrm{e}^{\mathrm{i}m\varphi}$.

The equation for Θ_{lm} can be solved through a power series expansion. For our purposes it is enough to note that there exist unique solutions if and only if $\ell \in \mathbb{N}_0$ and $|m| \leq \ell$. These solutions are then given by the associated Legendre polynomials $P_{lm}(\cos\vartheta)$ and by normalizing again in L^2 we have

$$\Theta_{lm}(\vartheta) = \sqrt{\frac{2\ell+1}{2} \cdot \frac{(\ell-m)!}{(\ell+m)!}} P_{lm}(\cos\vartheta)$$

Therefore the general spherical harmonics are given as the product

$$Y_{\ell m}(\vartheta,\varphi) = \Phi_m(\varphi)\Theta_{lm}(\vartheta) = \frac{1}{\sqrt{2\pi}}\sqrt{\frac{2\ell+1}{2} \cdot \frac{(\ell-m)!}{(\ell+m)!}} P_{lm}(\cos\vartheta)\mathrm{e}^{\mathrm{i}m\varphi}.$$

Proposition 19. *The spherical harmonics $Y_{\ell m}$ form a complete orthonormal system of functions in the Hilbert space $L^2(S^2)$ with respect to its canonical scalar product, which is to say that*

$$\int_{-\pi}^{\pi}\int_{0}^{\pi} \overline{Y_{\ell' m'}(\vartheta,\varphi)} Y_{\ell m}(\vartheta,\varphi)\ \sin\vartheta\,\mathrm{d}\vartheta\mathrm{d}\varphi = \delta_{ll'}\delta_{mm'}. \tag{2.2}$$

Proof. The proof of this is due to properties of the associated Legendre polynomials, namely the differential equations they satisfy. Again we refer the reader to [Duff and Naylor (1966)], Chapter 9, for details. □

An immediate consequence of this proposition is

Corollary 20. *Every function $f \in L^2(S^2)$ can be expanded in spherical harmonics as follows:*

$$f(\vartheta,\varphi) = \sum_{\ell=0}^{\infty}\sum_{m=-\ell}^{\ell} c_{lm} Y_{\ell m}(\vartheta,\varphi) \tag{2.3}$$

The expansion is to be understood in the sense of $L^2(S^2)$-convergence which means that

$$\lim_{N\to\infty} \int_{-\pi}^{\pi}\int_{0}^{\pi} \left| f(\vartheta,\varphi) - \sum_{\ell=0}^{N}\sum_{m=-\ell}^{\ell} c_{lm} Y_{\ell m}(\vartheta,\varphi)\right|^2 \sin\vartheta\,\mathrm{d}\vartheta\mathrm{d}\varphi = 0.$$

The coefficients c_{lm} can be obtained by multiplying equation (2.3) by the complex conjugate $\overline{Y_{\ell m}}$ of a spherical harmonic $Y_{\ell m}$ and then integrating over S^2 exploiting the orthonormality relations (2.2). This yields

$$c_{lm} = \int_{-\pi}^{\pi}\int_{0}^{\pi} \overline{Y_{\ell m}(\vartheta,\varphi)} f(\vartheta,\varphi)\sin\vartheta\,\mathrm{d}\vartheta\mathrm{d}\varphi.$$

It is also possible to expand functions f on the unit ball $B_1(0)$, i.e., $f \in L^2(B_1(0))$, by means of spherical harmonics, allowing the coefficients to depend on the radius r.

Definition 21. Let us introduce the following notation

$$V_\ell := \text{span}\{Y_{\ell m} \in L^2(S^2) | -\ell \leq m \leq \ell\}$$

and call the elements of V_ℓ spherical harmonics of degree ℓ. This is a $2\ell+1$-dimensional real vector space. Its elements are homogeneous polynomials in $\cos\vartheta$ of degree l.

Representation Theory

Now we want to use spherical harmonics to give a classification of the irreducible representations of the orthogonal group $O(3)$ on spaces of odd dimension, such as V_ℓ. This is relevant for the spherical Bénard problem because the governing equations obey an $O(3)$-symmetry. Since $O(3) = SO(3) \oplus \mathbb{Z}_2^c$ where $\mathbb{Z}_2^c := \{\pm\mathbb{1}\}$ we first determine all irreducible representations of $SO(3)$. For a proper derivation of the following two propositions that allow us to do so see [Golubitsky et al. (1988)], Chapter XIII, §7. We only prove the second one here.

Proposition 22. *The representation of $SO(3)$ on V_ℓ given through*

$$\gamma p(x) = p(\gamma^{-1}x) \quad \textit{where} \quad p \in V_\ell,\ \gamma \in SO(3)$$

is absolutely irreducible. In fact, every irreducible representation of $SO(3)$ is isomorphic to some V_ℓ.

The proof requires some more involved techniques from representation theory using properties of the characters of the representations. Based on this discovery we are able to classify the irreducible representations of $O(3)$.

Proposition 23. *The only irreducible representations of $O(3)$ are the representations on V_ℓ given by*

$$\begin{aligned} \gamma p(x) &= p(\gamma^{-1}x), \quad \gamma \in SO(3),\ p \in V_\ell \\ (-\mathbb{1})p(x) &= p(x) \end{aligned}$$

and

$$\begin{aligned} \gamma p(x) &= p(\gamma^{-1}x), \quad \gamma \in SO(3),\ p \in V_\ell \\ (-\mathbb{1})p(x) &= -p(x). \end{aligned}$$

Proof. Let V be any irreducible representation of $O(3)$. Decompose V into two eigenspaces for the action of $-\mathbb{1}$,

$$V = V_1 \oplus V_{-1},$$

where $-\mathbb{1}$ acts as the identity on V_1 and as minus the identity on V_{-1}. The two subspaces are invariant because $\mathbb{Z}_2^c$ commutes with $SO(3)$. So either $V = V_1$ or $V = V_{-1}$. In either case V is irreducible as a representation of $SO(3)$ and therefore isomorphic to some V_ℓ. Thus we obtain only the two types of representation listed above. □

The two representations are commonly called the plus and minus representations of $O(3)$ on V_ℓ. In applications $O(3)$ usually acts in the way that is induced from its natural action on $\mathbb{R}^3$, where $-\mathbb{1} \cdot (x,y,z) = (-x, -y, -z)$ is the reflexion through the origin. Therefore we let the non-trivial element in $\mathbb{Z}_2^c$ act on V_ℓ as the identity when ℓ is even and as minus the identity when ℓ is odd, since $p(-x, -y, -z) = (-1)^l p(x,y,z)$ for a homogeneous polynomial p of degree ℓ. We call this the **natural representation** of $O(3)$ on the space of spherical harmonics.

2.4 Center Manifold Reduction

In the following we introduce the concept of center manifold reduction. It poses a powerful method of reducing the dimension of the space we are working with while preserving all features of the original dynamical system that are important from a bifurcational point of view, in particular the existence and stability of solution branches. Our presentation of these results is based on [Kuznetsov (1995)], Chapter 5, and [Henry (1981)], Chapter 6.2, the latter only for the infinite-dimensional case.

It is well known that for a hyperbolic fixed point x_0 of a dynamical system $\dot{x} = f(x)$ the tangent space in this point decomposes into a stable and an unstable subspace, $T_{x_0} = T^s_{x_0} \oplus T^u_{x_0}$, corresponding to the eigenvalues of the Jacobian matrix $\mathrm{D}f_{(x_0)}$ with negative and positive real parts, respectively. We also know that there are unique local invariant manifolds tangent to $T^s_{x_0}$ and $T^u_{x_0}$ such that trajectories on these manifolds tend to x_0 for positive and negative times, respectively. We call these the stable ($W^s(x_0)$) and the unstable manifold ($W^u(x_0)$) of x_0. They are of the same dimension as the corresponding eigenspaces and of the same finite smoothness as f.

For a non-hyperbolic fixed point the Jacobian has at least one eigenvalue λ with $\mathrm{Re}(\lambda) = 0$. We call the corresponding generalized eigenspace $T^c_{x_0}$, the **center space**. Theorem 24 assures the existence of an invariant manifold for the system which is tangent to this space in x_0.

For now consider an autonomous system of the form

$$\dot{x} = f(x), \quad x \in \mathbb{R}^n \tag{2.4}$$

where f is sufficiently smooth and $f(0) = 0$. Suppose that the Jacobian $\mathrm{D}f_{(0)}$ has n_+ eigenvalues with real part $\mathrm{Re} > 0$, n_- eigenvalues with $\mathrm{Re} < 0$ and n_0 eigenvalues with $\mathrm{Re} = 0$, always counting multiplicities. Then we have $\dim(W^s(0)) = n_-$ and $\dim(W^u(0)) = n_+$.

Theorem 24 (Existence of Center Manifolds I)**.** *In the setting described above there exists a locally defined smooth invariant manifold $W^c_{loc}(0)$ of dimension n_0 that is tangent to T^c_0 at 0 and has the same finite smoothness as f.*

Definition 25. The manifold $W^c_{loc}(0)$ is called **center manifold**. We usually drop the "loc" to simplify notation and remember that it is just a locally defined object.

In contrast to the stable and unstable manifold the center manifold need not be unique as one can quickly verify through the following example: Consider the system

$$\begin{cases} \dot{x} &= x^2 \\ \dot{y} &= -y \end{cases},$$

for which $(0,0)$ is an equilibrium and note that several manifolds possessing the properties of a center manifold exist, namely

$$W^c_\alpha(0) := \{(x,y) \mid y = \phi_\alpha(x)\},$$

where $\alpha \in \mathbb{R}$ and

$$\phi_\alpha(x) := \begin{cases} \alpha \mathrm{e}^{\frac{1}{x}} & \text{for } x \leq 0 \\ 0 & \text{for } x \geq 0 \end{cases}.$$

Here the center space T^c_0 is the x-axis and the graph of ϕ_α is tangent to it at $(0,0)$. The set $W^c_\alpha(0)$ is indeed an invariant manifold because for any $(x,y) = (x,\alpha \mathrm{e}^{\frac{1}{x}}) \in W^c_\alpha(0)$ we calculate

$$\begin{pmatrix} \dot{x} \\ \dot{y} \end{pmatrix} = \begin{pmatrix} x^2 \\ -y \end{pmatrix} = \begin{pmatrix} x^2 \\ -\alpha \mathrm{e}^{\frac{1}{x}} \end{pmatrix} = x^2 \cdot \begin{pmatrix} 1 \\ -\frac{\alpha}{x^2} \mathrm{e}^{\frac{1}{x}} \end{pmatrix} = x^2 \cdot \begin{pmatrix} \frac{\partial}{\partial x} x \\ \frac{\partial}{\partial x} \alpha \mathrm{e}^{\frac{1}{x}} \end{pmatrix}.$$

The last term is clearly an element of the tangent space $T_{(x,y)} W^c_\alpha(0)$. So the trajectory through (x,y) stays on $W^c_\alpha(0)$ and therefore we have a center manifold $W^c_\alpha(0)$ for every $\alpha \in \mathbb{R}$.

Furthermore, note that the center manifold has the same *finite* smoothness as f. This does not imply that for $f \in C^\infty(\mathbb{R}^n,\mathbb{R}^n)$ there exists a C^∞-manifold since the neighborhood of existence may shrink to a single point with increasing smoothness.

The reason why these manifolds are of major interest is that they contain "the interesting part" of the dynamics in the sense that it suffices to project a system to its center manifold and analyze the dynamics of the projected equation. To see why this is the case we write system (2.4) in an eigenbasis (u,v) so that it takes the form

$$\begin{cases} \dot{u} &= Bu + g(u,v) \\ \dot{v} &= Cv + h(u,v) \end{cases}, \tag{2.5}$$

where B is a matrix with all its eigenvalues on the imaginary axis and C has no eigenvalues there. Of course, then $u \in \mathbb{R}^{n_0}$ and $v \in \mathbb{R}^{n_+ + n_-}$ for dimensional reasons. Also $g(u,v) =$

$O(\|(u,v)\|^2)$ and the same holds for h. Locally it is then possible to write the center manifold as the graph of a smooth function $F : \mathbb{R}^{n_0} \to \mathbb{R}^{n_+ + n_-}$

$$W^c(0) = \{(u,v) \mid v = F(u)\},$$

where $\mathrm{D}F_{(0)} = 0$ and $F(0) = 0$ since $W^c(0)$ is tangent to T_0^c. Now we can state

Theorem 26. *Maintaining the notation from above system (2.5) is locally topologically equivalent to*

$$\begin{cases} \dot{u} &= Bu + g(u,F(u)) \\ \dot{v} &= Cv \end{cases} . \tag{2.6}$$

It is essential to note that the equations in Theorem 26 are uncoupled and the first equation is simply the restriction of the system to its center manifold. From this form it is clear that the local dynamical behavior of the entire system depends only on the dynamics on the center manifold since the rest is easily described: Solutions of the second equation either grow or decay exponentially in time depending on nothing more but the real part of the corresponding eigenvalue. The complex behavior is therefore isolated within the first equation. If the center manifold is not unique, the restrictions to all possible choices for $W^c(0)$ are topologically equivalent.

Since no eigenvalues of C lie on the imaginary axis we can split the second equation of (2.6) into an expanding and a contracting part:

$$\begin{cases} \dot{v} &= -v \quad v \in \mathbb{R}^{n_-} \\ \dot{w} &= w \quad w \in \mathbb{R}^{n_+} \end{cases}$$

These are the equations of a standard saddle which provides us with the following neat way to rephrase Theorem 26: For a non-hyperbolic equilibrium the system is locally topologically equivalent to the suspension of its restriction to the center manifold by the standard saddle.

We now introduce k parameters into our system which brings us closer to the setting in which we actually want to apply the center manifold methods and does not pose much additional difficulty. For

$$\dot{x} = f(x,\mu), \quad x \in \mathbb{R}^n,\ \mu \in \mathbb{R}^k \tag{2.7}$$

with $f(x_0,\mu_0) = 0$ consider the extended system

$$\begin{cases} \dot{x} = f(x,\mu) \\ \dot{\mu} = 0 \end{cases} \tag{2.8}$$

or again in an eigenbasis

$$\begin{cases} \dot{u} &= B_\mu u + g_\mu(u,v) \\ \dot{v} &= C_\mu v + h_\mu(u,v) \\ \dot{\mu} &= 0 \end{cases} . \tag{2.9}$$

Then the Jacobian of (2.9) has $n_0 + k$ eigenvalues on the imaginary axis. Theorem 24 therefore guarantees the existence of an $n_0 + k$-dimensional center manifold W^c that is tangent to the μ-space and also to the eigenspace spanned by the eigenvectors of B. Since $\dot{\mu} = 0$ the subspaces $\Pi_{\mu_0} := \{(x,\mu) \mid \mu = \mu_0\}$ are invariant and thus we can think of the center manifold as being foliated by n_0-dimensional invariant manifolds W^c_μ of the form

$$W^c_\mu = W^c \cap \Pi_\mu.$$

Note that W^c_0 is precisely the center manifold of the parameter-independent system (2.6). Now letting $|\mu|$ be sufficiently small we restrict the system to W^c_μ and choose coordinates $u \in \mathbb{R}^{n_0}$ on W^c_μ by projecting W^c_μ onto T^c. This can be done for small $|\mu|$ since the center manifold is tangent to T^c. This restriction is then given by a smooth system

$$\dot{u} = F(u,\mu) \tag{2.10}$$

and in complete analogy to the parameter-independent case our original system (2.8) is topologically equivalent to the suspension of (2.10) by the standard saddle. This implies that the dynamics near a bifurcation point (x_0,μ_0) are determined by the dynamics on the $n_0 + k$-dimensional center manifold of system (2.8). Note that this manifold has the favorable property of being independent of the parameter μ. Of course we could also consider μ-dependent manifolds for system (2.7) without introducing the extended system.

Now that we know theoretically how to reduce the dimension of the system under investigation in order to analyze the local dynamics the next step is to compute the function F determining the center manifold and thus the "reduced" vector field given through system (2.6) that is topologically equivalent to our original system.
We can neglect the parameter μ in the computation because the dynamics are governed by the behavior of the extended system on its (μ-independent) center manifold. So it suffices to compute the relevant Taylor coefficients of F for the parameter-independent case up to a certain order. [Kuznetsov (1995)] explains in Chapter 5.4 how this can be done by hand, determining one coefficient at a time in recursive fashion where each time we have to solve a linear system of algebraic equations. The coefficients calculated in this way are the same for all center manifolds in case there is more than one.

Let us consider another example to see that the linear approximation of the center manifold, i.e., to simply project the system onto T^c, is not always sufficient to answer stability

questions. Consider the system

$$\begin{cases} \dot{x} = xy + x^3 \\ \dot{y} = -y - 2x^2 \end{cases} . \tag{2.11}$$

There is an equilibrium at $(0,0)$ and the linearization at this point is

$$A_{(0,0)} = \begin{pmatrix} 0 & 0 \\ 0 & -1 \end{pmatrix}$$

with eigenvalues 0 and -1. The center space is therefore one-dimensional, namely

$$T^c = \{(x, 0) \mid x \in \mathbb{R}\}.$$

So the projection of system (2.11) to T^c reads $\dot{x} = x^3$ and therefore we might expect the equilibrium to be unstable. However, this turns out to be false: A relatively simple computation, cf. [Kuznetsov (1995)], page 153, shows that the second order approximation of the function F determining the center manifold looks like

$$F(x) = -2x^2 + O(x^3)$$

and therefore in accordance with (2.6) the projection to this manifold yields

$$\dot{x} = xF(x) + x^3 = -2x^3 + x^3 + O(x^4) = -x^3 + O(x^4),$$

which shows that in contrast to what our first hasty guess suggested the equilibrium is actually stable.
In general it is not necessary to transform the system into an eigenbasis to compute the coefficients of F. [Kuznetsov (1995)] introduces a functional analytic projection method which enables us to avoid this disadvantage.

The methods explained in this chapter are crucial for the analysis of the spherical Bénard problem because a center manifold reduction restricts the problem to a low-dimensional space where the examination of the local dynamics is still complex but much more accessible. However, there is one more obstacle we have to overcome if we want to use the results described in this section for our purposes: The Bénard problem is posed on an infinite-dimensional space, namely the space of L^2-functions defined on a spherical gap, but everything we have learned about center manifolds so far can only be applied in finite-dimensional settings. As a matter of fact it is possible to generalize these results and to finish this chapter we cite a more general theorem on the existence of center manifolds which is valid for Banach spaces and can be found (including proof) in [Henry (1981)], Chapter 6.2. Although some new terms come up which we loosely explain below note that the essence of Theorem 27 is the same as what we had for $\mathbb{R}^n$ in Theorem 24.

Theorem 27 (Existence of Center Manifolds II)**.** *Let X be a Banach space and $A : X \to X$ a sectorial operator. Suppose that $0 \leq \alpha < 1$ and U is a neighborhood of 0 in X^α. Consider a C^1-function $h : U \to X$ with $h(0) = 0$. We analyze the equation*

$$\dot{x} = -Ax + h(x)$$

which has 0 as a trivial solution. Set $L := A - h'(0)$ and assume that L has no eigenvalues in the left half plane and that $\sigma(L) \cap \mathrm{i}\mathbb{R}$ is a spectral set. Then the following is true:

- *X decomposes into L-invariant subspaces $X = X_1 \oplus X_2$ such that $\mathrm{Re}(\sigma(L_1)) = 0$ and $\mathrm{Re}(\sigma(L_2)) > 0$ where $L_i := L\,|_{X_i}$.*
- *There exists a local invariant manifold $W^c(0) = \{x_1 + F(x_1) \mid x_1 \in X_1, \|x_1\| < \delta\}$ that is tangent to X_1 at the origin.*
- *The stability of the trivial solution in X^α is determined by its stability in $W^c(0)$ and the flow in $W^c(0)$ is governed by the ordinary differential equation*

  $$\dot{x}_1 = -L_1 x_1 + E_1 g(x_1 + F(x_1))$$

  where $g(x) := h(x) - h'(0)x$ and E_1 is the projection of X onto X_1.

Furthermore, if X_1 is finite-dimensional and $h \in C^k$ then there exists a unique polynomial function ϕ of order k such that $\|F(x) - \phi(x)\|_\alpha = O(\|x\|^k)$ as $x \to 0$ in X_1. Thus the center manifold is of the same smoothness as h.

Even though we do not present the proof of this theorem here let us take a closer look at some of the conditions and indicate the role that they play. References to theorems and definitions in the next paragraph all refer to [Henry (1981)].

The term **sectorial** denotes a property of a closed linear operator on a Banach space, a certain condition posed on its resolvent set. We do not want to make it explicit here (see Definition 1.3.1) but note that together with the fact that $\sigma(L) \cap \mathrm{i}\mathbb{R}$ is a spectral set this implies the decomposition of X into L-invariant subspaces, which follows from Theorem 1.5.2. Here a set $\sigma \subset \sigma(L) \cup \{\infty\}$ is called **spectral** if both σ and its complement are closed subsets of the extended plane $\mathbb{C} \cup \{\infty\}$, cf. Definition 1.5.1.
Finally let us state that $X^\alpha \subset X$ is a continuously embedded dense subspace of X, dependent on the operator A. The continuity of this embedding holds with respect to the norm $\|.\|_\alpha$ as introduced in Definition 1.4.7 and is proved in Theorem 1.4.8. So much for a brief overview of the theory around this result.

This version of the center manifold theorem enables us to use center manifold theory in an infinite-dimensional setting. In the spherical Bénard problem the center space X_1 is always finite-dimensional so smoothness of the center manifold will not be an issue. As we discuss in section 3.3 the system generically reduces to a $2\ell + 1$-dimensional space of spherical harmonics.

3 The Spherical Bénard Problem

The central chapter of this thesis deals with the spherical Bénard problem as it was introduced at the beginning of this work: We consider an incompressible fluid that is confined between two concentric spheres where the inner sphere is uniformly heated and a radial force field is imposed upon the domain. The governing equations are then invariant under the natural action of the orthogonal group $O(3)$. After discussing the system of equations and appropriate boundary conditions in the first section of this chapter we expand the solution in spherical harmonics and investigate the nature of the bifurcation that corresponds to the onset of convection. In the last two sections we introduce the concept of mode interaction and look for heteroclinic connections between equilibria.

3.1 Equations and Boundary Conditions

In this section we introduce the system of equations that govern the spherical Bénard problem and explain their various parameters. We also discuss appropriate boundary conditions. In doing so we proceed along the lines of [Chandrasekhar (1961)], Chapter VI, §55-§56, unless explicitly stated otherwise.

Equations and Parameters

We assume that the fluid is incompressible which means that its volume does not change in response to a pressure change. Therefore we have $\frac{\partial \rho}{\partial t} = 0$ for the density ρ of the fluid. Together with the continuity equation

$$\frac{\partial \rho}{\partial t} + \operatorname{div}(\rho u) = 0$$

this yields

$$\operatorname{div} u = 0 \tag{3.1}$$

for the velocity field u. Such divergence-free vector fields are sometimes also called **solenoidal**. Now according to [Travnikov et al. (2003)] the Navier-Stokes equations for incompressible flow in their Boussinesq approximation and the energy equation take the following form

$$\rho \left[\frac{\partial u}{\partial t} + \langle u, \nabla \rangle u \right] = -\nabla p + \rho \nu \Delta u + f \tag{3.2}$$

$$\frac{\partial T}{\partial t} + \langle u, \nabla T \rangle = \kappa \Delta T. \tag{3.3}$$

Table 3.1: Variables and parameters

Symbol	Unit	Dim	Meaning
x	m	3	position
u	m/s	3	velocity field
p	Pa	1	pressure distribution
T	K	1	temperature distribution
θ	K	1	temperature perturbation
ρ	kg/m^3	1	density of the fluid
g	$1/\mathrm{s}^2$	1	coefficient of the radial gravitational field $g(r)x$
α	$1/\mathrm{K}$	1	coefficient of volume expansion
ν	m^2/s	1	coefficient of kinematic viscosity
κ	m^2/s	1	coefficient of thermal diffusivity
A	J/sm^3	1	rate of heat generation
c_P	J/kgK	1	specific heat of the fluid

The meaning of the quantities and parameters that come up in the equations is listed in Table 3.1. The body force term f is made precise below. In order to perform a linear stability analysis we introduce the perturbation quantities $u = U + u'$ and $T = \tilde{T} + \theta$ where u' and θ are deviations from the basic state $(U,\tilde{T})$. But of course the basic state is pure heat conduction without fluid movement, so $U \equiv 0$ and thus $u' = u$. We plug this into equations (3.2) and (3.3), divide (3.2) by ρ and write T instead of $\tilde{T}$ again. Then we neglect all the terms that are nonlinear in the perturbation quantities to obtain

$$\frac{\partial u}{\partial t} = -\rho^{-1}\nabla p + \tilde{f} + \nu\Delta u \tag{3.4}$$

$$\frac{\partial \theta}{\partial t} = -\langle u,\nabla T\rangle + \kappa\Delta\theta. \tag{3.5}$$

According to [Chandrasekhar (1961)], Chapter VI, §56, the radially symmetric radial gravitational field $g(r)x$ determines the body force term $\tilde{f}$ to be

$$\tilde{f} = \alpha g(r)\theta x$$

which we abbreviate by

$$\gamma(r)\theta x.$$

The Temperature Distribution

Let us now discuss the form of the initial temperature gradient ∇T. Suppose that a distribution of heat sources within the domain constantly generates heat at a rate A. According to Chapter 7.2 of [Fowler (2008)] the heat equation then yields

$$\kappa\Delta T = -\epsilon + \frac{\partial T}{\partial t} \qquad \text{where} \qquad \epsilon = \frac{A}{\rho c_P}. \tag{3.6}$$

Assume that ϵ is constant and the basic temperature distribution is independent of time, i.e., $\frac{\partial T}{\partial t} = 0$. Then (3.6) reduces to

$$\kappa \Delta T = -\epsilon$$

and we obtain a solution of the form

$$T(r) = \beta_0 - \beta_2 r^2 + \frac{\beta_1}{r}$$

where $\beta_2 = \frac{\epsilon}{6\kappa}$ and β_0, β_1 are real constants. We then define

$$\beta(r) := \beta_2 + \frac{\beta_1}{2r^3}$$

and obtain

$$\frac{\partial T}{\partial x_i} = -2\beta_2 x_i - \frac{\beta_1 x_i}{r^3} = -2\beta(r)x_i.$$

This means that the temperature gradient is of the form $\nabla T = -2\beta(r)x$. These considerations transform equations (3.4) and (3.5) into

$$\frac{\partial u}{\partial t} = -\rho^{-1}\nabla p + \gamma(r)\theta x + \nu \Delta u \tag{3.7}$$

$$\frac{\partial \theta}{\partial t} = 2\beta(r)\langle u, x\rangle + \kappa \Delta \theta. \tag{3.8}$$

It is our aim to study equations (3.1), (3.7) and (3.8) with respect to bifurcations and the stability of conductive and convective flow states. The conductive solution $u \equiv 0$ is a solution for any set of parameter values, in particular for any Rayleigh number C_ℓ, which is properly defined in equation (3.27). Physics tells us that for small C_ℓ this solution is stable but as the temperature gradient is increased it suddenly loses its stability and convection begins. The existence of this bifurcation is suspected from experiment data and physical reasoning and we want to discover it also in the mathematical formulation of the problem. The bifurcation type (Hopf or steady-state) determines the structure of the evolving flow patterns (stationary or periodic) that are stable after the bifurcation occurs. Before we begin our bifurcation analysis we perform a few elementary calculations to bring the equations into a more accessible form.

Elimination of the pressure term

We start by eliminating the pressure term ∇p from the equations. To this end we consider the vorticity ω, which is the curl of the velocity field, so $\omega := \text{curl}(u) = \nabla \times u$ and find

$$\begin{aligned}
\frac{\partial \omega_i}{\partial t} &= \frac{\partial}{\partial t}\left[\epsilon_{ijk}\frac{\partial}{\partial x_j}u_k\right] \\
&= \epsilon_{ijk}\frac{\partial}{\partial x_j}\frac{\partial}{\partial t}u_k \\
&= \epsilon_{ijk}\frac{\partial}{\partial x_j}\left[-\frac{\partial}{\partial x_k}\left(\frac{p}{\rho}\right) + \alpha g(r)\theta x_k + \nu\Delta u_k\right] \\
&= \underbrace{-\epsilon_{ijk}\frac{\partial^2}{\partial x_j \partial x_k}\left(\frac{p}{\rho}\right)}_{=0} + \epsilon_{ijk}\frac{\partial}{\partial x_j}\left[\gamma(r)\theta x_k\right] + \nu\epsilon_{ijk}\frac{\partial}{\partial x_j}\Delta u_k \\
&= \underbrace{\epsilon_{ijk}\frac{x_j}{r}\frac{\partial\gamma(r)}{\partial r}\theta x_k}_{=0} + \epsilon_{ijk}\gamma(r)\frac{\partial\theta}{\partial x_j}x_k + \nu\Delta\left[\epsilon_{ijk}\frac{\partial}{\partial x_j}u_k\right] \\
&= \gamma(r)\epsilon_{ijk}\frac{\partial\theta}{\partial x_j}x_k + \nu\Delta\omega_i
\end{aligned} \tag{3.9}$$

where we use equation (3.7) for the third equality and the rest is just straightforward calculation. Our notation is to be understood in the sense of the Einstein summation convention, i.e., summing over all indices that appear twice in a single term. It is also worth mentioning that we express the vector product $\times$ in three dimensions by making use of the Levi-Civita symbol:

$$\epsilon_{ijk} = \begin{cases} 1 & \text{if } (i,j,k) \text{ is an even permutation of } (1,2,3) \\ -1 & \text{if } (i,j,k) \text{ is an odd permutation of } (1,2,3) \\ 0 & \text{if two of the indices are equal} \end{cases}$$

For a further transformation of the equations we then take the curl again and use the vector calculus identity

$$\nabla \times (\nabla \times v) = \nabla \text{div}\, v - \Delta v \quad \text{(for any vector field } v\text{)}$$

where the Laplacian is to be taken in each component. Because the velocity field u is solenoidal this gives us

$$\begin{aligned}
\Delta u_i &= -(\nabla \times (\nabla \times u))_i \\
&= -(\nabla \times \omega)_i \\
&= -\epsilon_{ijk}\frac{\partial}{\partial x_j}\omega_k
\end{aligned}$$

and therefore using (3.9) for the second equality we have

$$\begin{aligned}
\frac{\partial}{\partial t}\Delta u_i &= -\epsilon_{ijk}\frac{\partial}{\partial x_j}\frac{\partial \omega_k}{\partial t} \\
&= -\epsilon_{ijk}\frac{\partial}{\partial x_j}\left[\gamma(r)\epsilon_{klm}\frac{\partial\theta}{\partial x_l}x_m + \nu\Delta\omega_k\right] \\
&= -\underbrace{\left[\epsilon_{ijk}\frac{\partial}{\partial x_j}\gamma(r)\epsilon_{klm}\frac{\partial}{\partial x_l}x_m\right]}_{=:L_i}\theta - \epsilon_{ijk}\frac{\partial}{\partial x_j}\nu\Delta\omega_k \\
&= -L_i\theta - \nu\Delta\epsilon_{ijk}\frac{\partial}{\partial x_j}\omega_k \\
&= -L_i\theta - \nu\Delta\Big[-\Delta u_i + \frac{\partial}{\partial x_i}\underbrace{(\text{div } u)}_{=0}\Big] \\
&= -L_i\theta + \nu\Delta^2 u_i. \qquad (3.10)
\end{aligned}$$

Now ω is solenoidal as well and we have $\langle x,\Delta v\rangle = \Delta\langle x,v\rangle$ for any v with div $v = 0$ where $\langle\,\cdot\,,\,\cdot\,\rangle$ is the standard scalar product. Therefore, using (3.9) again we get

$$\begin{aligned}
\frac{\partial}{\partial t}\langle x,\omega\rangle &= x_i\left[\gamma(r)\epsilon_{ijk}\frac{\partial\theta}{\partial x_j}x_k + \nu\Delta\omega_i\right] \\
&= \nu\Delta\langle x,\omega\rangle + \gamma(r)\underbrace{\left[x_i\epsilon_{ijk}\frac{\partial\theta}{\partial x_j}x_k\right]}_{=0} \\
&= \nu\Delta\langle x,\omega\rangle.
\end{aligned}$$

In the long run it is our goal to exploit the spherical geometry of the domain on which our problem is posed. The next lemma shows where the spherical harmonics enter the stage again.

Lemma 28. *The differential operator L_i satisfies the following equation:*

$$\sum_{i=1}^{3} x_i L_i = \gamma(r)\Delta_{\vartheta,\varphi}$$

Proof. The proof is a rather cumbersome calculation, we mention the important steps here. Expanding the cross product notation in L_i we find

$$\begin{aligned}
L_i &= \epsilon_{ijk}\frac{\partial}{\partial x_j}\gamma(r)\epsilon_{klm}\frac{\partial}{\partial x_l}x_m \\
&= \gamma(r)\left(\frac{\partial}{\partial x_i} + \frac{\partial}{\partial x_i}x_j\frac{\partial}{\partial x_j} - x_i\Delta\right) + \frac{1}{r}\frac{\partial\gamma(r)}{\partial r}\left(r^2\frac{\partial}{\partial x_i} - x_i x_j\frac{\partial}{\partial x_j}\right).
\end{aligned}$$

As one quickly sees the term including the derivative of γ vanishes if we multiply by x_i and sum over i. Note that there already is a summation over j, expressed through the Einstein convention. Therefore we are left with

$$\sum_{i=1}^{3} x_i L_i = \gamma(r) \sum_{i=1}^{3} \left(x_i \frac{\partial}{\partial x_i} + x_i \frac{\partial}{\partial x_i} x_j \frac{\partial}{\partial x_j} - x_i^2 \Delta \right).$$

Now we transform everything into polar coordinates and with

$$\sum_{i=1}^{3} x_i \frac{\partial}{\partial x_i} = r \frac{\partial}{\partial r}$$

we find

$$\begin{aligned} \sum_{i=1}^{3} x_i L_i &= \gamma(r) \left(r \frac{\partial}{\partial r} + r \frac{\partial}{\partial r} r \frac{\partial}{\partial r} - r^2 \Delta \right) \\ &= r^2 \gamma(r) \left(\frac{\partial^2}{\partial r^2} + \frac{2}{r} \frac{\partial}{\partial r} - \Delta \right) \\ &= \gamma(r) \Delta_{\vartheta,\varphi} \end{aligned}$$

which completes the proof. Note that we encounter again the operator $\Delta_{\vartheta,\varphi}$ from section 2.3, the angular portion of the Laplacian with the spherical harmonics $Y_{\ell m}$ as its eigenfunctions. □

Lemma 28 helps us to transform our equations so that we can make use of the spherical geometry of the domain. By the same argument as above (u being solenoidal) and using equation (3.10) we calculate

$$\begin{aligned} \gamma(r) \Delta_{\vartheta,\varphi} \theta &= \sum_{i=1}^{3} x_i L_i \theta \\ &= \sum_{i=1}^{3} x_i (\nu \Delta^2 u_i - \frac{\partial}{\partial t} \Delta u_i) \\ &= \nu \Delta^2 \langle u,x \rangle - \frac{\partial}{\partial t} \Delta \langle u,x \rangle. \end{aligned}$$

After all these transformation we finally obtain as the basic equations of our problem:

$$\frac{\partial \theta}{\partial t} = 2\beta(r) \langle u,x \rangle + \kappa \Delta \theta \tag{3.11}$$

$$\frac{\partial}{\partial t} \langle x,\omega \rangle = \nu \Delta \langle x,\omega \rangle \tag{3.12}$$

$$\gamma \Delta_{\vartheta,\varphi} \theta = \nu \Delta^2 \langle u,x \rangle - \frac{\partial}{\partial t} \Delta \langle u,x \rangle \tag{3.13}$$

Note that we have now achieved that the only terms where the velocity field u and the vorticity ω occur are their respective scalar products with the position x. This version of the perturbation equations for our problem enables us to expand suitable expressions in spherical harmonics and in this way reduce the system to one of ordinary differential equations.

Boundary Conditions

Let us measure length in units of the radius R_2 of the outer shell. Then the domain is confined between two concentric spherical shells of radius $\eta = \frac{R_1}{R_2}$ and 1, respectively. Now as boundary conditions we must have

$$\theta(\eta) = \theta(1) = 0 \tag{3.14}$$

where we use the abbreviation

$$\theta(\eta) = \theta(x)\big|_{\{x \mid \|x\|=\eta\}}.$$

Furthermore, it is certainly reasonable to demand that the radial component of the velocity field $u = (u_r,u_\vartheta,u_\varphi)$ also vanishes at the boundaries which means

$$u_r(\eta) = u_r(1) = 0. \tag{3.15}$$

For the remaining boundary condition it is essential to consider the nature of the surfaces at $r = 1$ and $r = \eta$. In this work we assume both boundaries to be rigid rather than free, as is (approximately) the case at the inner core/outer core, outer core/mantle and mantle/crust boundaries inside the Earth. Therefore the transverse components of the velocity field need to vanish at the boundary, so

$$u_\vartheta(\eta) = u_\vartheta(1) = u_\varphi(\eta) = u_\varphi(1) = 0. \tag{3.16}$$

Taking into account that the velocity field is solenoidal we find

$$\begin{aligned} 0 &= [\text{div } u]_{r=1,\eta} \\ &= \left[\frac{\partial u_r}{\partial r} + 2\frac{u_r}{r} + \frac{1}{r}\frac{\partial u_\vartheta}{\partial \vartheta} + \frac{\cos\vartheta}{\sin\vartheta}\frac{u_\vartheta}{r} + \frac{1}{r\sin\vartheta}\frac{\partial u_\varphi}{\partial \varphi}\right]_{r=1,\eta} \\ &= \left[\frac{\partial u_r}{\partial r} + \frac{1}{r}\frac{\partial u_\vartheta}{\partial \vartheta} + \frac{1}{r\sin\vartheta}\frac{\partial u_\varphi}{\partial \varphi}\right]_{r=1,\eta} \\ &= \left.\frac{\partial u_r}{\partial r}\right|_{r=1,\eta} \end{aligned} \tag{3.17}$$

where the third equality holds because of (3.15) and (3.16). The fourth equality is due to the fact that for constant $r = 1$ or $r = \eta$ the angular components of the velocity vanish everywhere, so the same goes for their respective angular derivatives.

3.2 Expansion in Spherical Harmonics

The content of this section is discussed in [Chandrasekhar (1961)], Chapter VI, §56, in a more condensed way. We have seen in section 2.3 that spherical harmonics and their properties are intrinsically related to the structure of the sphere in three-dimensional space. Exploiting the spherical geometry of our domain it is now suitable to expand the solution –

or rather the radial components of u and ω – in spherical harmonics. We do not address the smoothness of the solution here. Suffice it to say that if u is a classical solution then its radial component is certainly an L^2-function and can therefore be expanded in spherical harmonics.

To this end we write $u = (u_r,u_\vartheta,u_\varphi)$, where $u_r(x)$ is the projection of $u(x)$ to the radial straight line through x and the angular components $u_\vartheta(x)$ and $u_\varphi(x)$ are the deviations of $u(x)$ from the radial vector through x in the respective angular directions as sketched in Figure 3.1 for two dimensions. The vector field ω is transformed accordingly. We implement the time dependence of the velocity field u by an exponential term in t with an appropriate coefficient for each summand in the expansion. In these coordinates we write:

$$\langle x,\omega\rangle = r\omega_r = \sum_{\ell=0}^{\infty}\sum_{m=-\ell}^{\ell} Z_{\ell m}(r)Y_{\ell m}(\vartheta,\varphi)\mathrm{e}^{p_{\ell m}t} \tag{3.18}$$

$$\langle x,u\rangle = ru_r = \sum_{\ell=0}^{\infty}\sum_{m=-\ell}^{\ell} W_{\ell m}(r)Y_{\ell m}(\vartheta,\varphi)\mathrm{e}^{p_{\ell m}t} \tag{3.19}$$

$$\theta = \sum_{\ell=0}^{\infty}\sum_{m=-\ell}^{\ell} \Theta_{\ell m}(r)Y_{\ell m}(\vartheta,\varphi)\mathrm{e}^{p_{\ell m}t} \tag{3.20}$$

We now have to determine the coefficients $Z_{\ell m},W_{\ell m},\Theta_{\ell m}$ of these expansions for $r \in [\eta, 1]$.

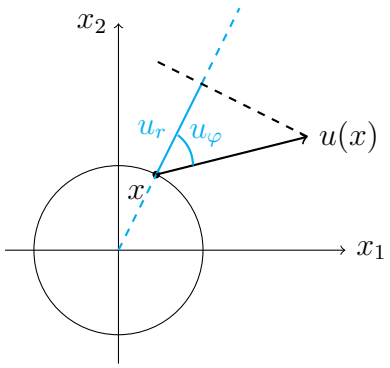

Figure 3.1: Coordinates

The exponents $p_{\ell m}$ determine the stability of the trivial solution by the sign of their real part and in this way correspond to the eigenvalues of the linearization of the right hand side of the system. For the sake of readability we usually drop the indices and simply write $Z(r)$ instead of $Z_{\ell m}(r)$ and accordingly for W, Θ and p as long as this causes no confusion. As we know from section 2.3

$$\Delta = \frac{\partial^2}{\partial r^2} + \frac{2}{r}\frac{\partial}{\partial r} - \frac{\Delta_{\vartheta,\varphi}}{r^2}$$

holds, and therefore for a function f of r only we have

$$\begin{aligned}\Delta(Y_{\ell m}(\vartheta,\varphi)f(r)) &= Y_{\ell m}(\vartheta,\varphi)\left[\frac{\partial^2}{\partial r^2}+\frac{2}{r}\frac{\partial}{\partial r}\right]f(r)-\frac{f(r)}{r^2}\Delta_{\vartheta,\varphi}Y_{\ell m}(\vartheta,\varphi)\\ &= Y_{\ell m}(\vartheta,\varphi)\left[\frac{\mathrm{d}^2}{\mathrm{d}r^2}+\frac{2}{r}\frac{\mathrm{d}}{\mathrm{d}r}\right]f(r)-\frac{\ell(\ell+1)}{r^2}f(r)Y_{\ell m}(\vartheta,\varphi)\\ &= Y_{\ell m}(\vartheta,\varphi)\mathcal{D}_\ell f(r)\end{aligned}$$

with the differential operator

$$\mathcal{D}_\ell=\frac{\mathrm{d}^2}{\mathrm{d}r^2}+\frac{2}{r}\frac{\mathrm{d}}{\mathrm{d}r}-\frac{\ell(\ell+1)}{r^2}.$$

As already mentioned earlier we measure length in units of the outer radius R_2 which means we set "$r=\frac{r}{R_2}$" in the equations. Inserting the expansion into the previous equations (3.11) to (3.13) we obtain a system of ordinary differential equations in the coefficient functions Z, W and Θ:

$$(\mathcal{D}_\ell-\mathcal{P}\sigma)\Theta(r) = -\frac{2\beta}{\kappa}R_2^2W(r) \tag{3.21}$$

$$(\mathcal{D}_\ell-\sigma)Z(r) = 0 \tag{3.22}$$

$$\mathcal{D}_\ell(\mathcal{D}_\ell-\sigma)W(r) = \frac{\gamma}{\nu}R_2^4\ell(\ell+1)\Theta(r) \tag{3.23}$$

Here we have set $\sigma:=\frac{pR_2^2}{\nu}$ and $\mathcal{P}:=\frac{\nu}{\kappa}$ is the dimensionless Prandtl number, proportional to the kinematic viscosity and reciprocally proportional to the thermal diffusivity of the fluid. Transforming partial differential equations into ordinary ones is certainly a qualitative simplification of the problem, but note that there are now infinitely many ordinary differential equations since $\ell\in\mathbb{N}$ and $|m|\le\ell$. The boundary conditions (3.14) and (3.15) convert to

$$W(\eta)=W(1)=\Theta(\eta)=\Theta(1)=0 \tag{3.24}$$

and (3.17) is equivalent to

$$\left.\frac{\mathrm{d}W}{\mathrm{d}r}\right|_{r=1,\eta}=0. \tag{3.25}$$

The Velocity Field

Suppose now we have found a solution of equations (3.21) to (3.23). To solve our original problem it is then necessary to determine from this the remaining components of the velocity field u_ϑ and u_φ. This is done using a general characterization of solenoidal vector fields for which we need the following definition.

Definition 29. Let $\Phi,\Psi:\mathbb{R}^3\to\mathbb{R}$ be arbitrary scalar functions. A vector field $\mathbf{T}$ of the form $\mathbf{T}=\nabla\times\Psi\mathbf{r}$ where $\mathbf{r}$ is the radial unit vector in spherical coordinates is called **toroidal** with defining scalar Ψ. Similarly, a vector field $\mathbf{S}$ of the form $\mathbf{S}=\nabla\times(\nabla\times\Phi\mathbf{r})$ is called **poloidal** with defining scalar Φ.

After an appropriate transformation into spherical coordinates the gradient ∇ takes the following form

$$\nabla = \begin{pmatrix} \frac{\partial}{\partial r} \\ \frac{1}{r}\frac{\partial}{\partial \vartheta} \\ \frac{1}{r\sin\vartheta}\frac{\partial}{\partial \varphi} \end{pmatrix}$$

and the curl operator transforms to

$$\nabla \times \begin{pmatrix} a_r \\ a_\vartheta \\ a_\varphi \end{pmatrix} = \begin{pmatrix} \frac{1}{r\sin\vartheta}\left(\frac{\partial}{\partial\vartheta}(a_\varphi \sin\vartheta) - \frac{\partial a_\vartheta}{\partial\varphi}\right) \\ \frac{1}{r}\left(\frac{1}{\sin\vartheta}\frac{\partial a_r}{\partial\varphi} - \frac{\partial}{\partial r}(r a_\varphi)\right) \\ \frac{1}{r}\left(\frac{\partial}{\partial r}(r a_\vartheta) - \frac{\partial a_r}{\partial\vartheta}\right) \end{pmatrix}.$$

This enables us to calculate the coordinates of a toroidal field $\mathbf{T}$ in dependence of its defining scalar Ψ.

$$\mathbf{T} = \begin{pmatrix} T_r \\ T_\vartheta \\ T_\varphi \end{pmatrix} = \nabla \times \Psi\mathbf{r} = \nabla \times \begin{pmatrix} \Psi \\ 0 \\ 0 \end{pmatrix} = \begin{pmatrix} 0 \\ \frac{1}{r\sin\vartheta}\frac{\partial\Psi}{\partial\varphi} \\ -\frac{1}{r}\frac{\partial\Psi}{\partial\vartheta} \end{pmatrix}$$

In the same way we obtain the components of $\mathbf{S}$ in dependence of Φ.

$$\mathbf{S} = \begin{pmatrix} S_r \\ S_\vartheta \\ S_\varphi \end{pmatrix} = \nabla \times (\nabla \times \Phi\mathbf{r}) = \nabla \times \begin{pmatrix} 0 \\ \frac{1}{r\sin\vartheta}\frac{\partial\Phi}{\partial\varphi} \\ -\frac{1}{r}\frac{\partial\Phi}{\partial\vartheta} \end{pmatrix} = \begin{pmatrix} -\frac{1}{r^2}\Delta_{\vartheta,\varphi}\Phi \\ \frac{1}{r}\frac{\partial^2\Phi}{\partial r\partial\vartheta} \\ \frac{1}{r\sin\vartheta}\frac{\partial^2\Phi}{\partial r\partial\varphi} \end{pmatrix}$$

The next proposition shows that we can always express a solenoidal vector field as the sum of toroidal and poloidal fields, in other words a solenoidal field is given by two defining scalar functions.

Proposition 30. *Every solenoidal vector field v on $B_1(0)$ can be decomposed into a toroidal and a poloidal part, i.e., such a vector field is determined by two scalar functions Φ and Ψ by means of*

$$v = \underbrace{(\nabla \times \Psi\mathbf{r})}_{F} + \underbrace{(\nabla \times (\nabla \times \Phi\mathbf{r}))}_{G}$$

This is known as the Mie representation theorem, it is stated and proved in the paper of [Backus (1986)] on page 87. Since the velocity field u is a solenoidal vector field this enables us to write

$$u = F + G$$

where F is toroidal and G is poloidal. So the problem of determining the remaining components of the velocity field reduces to calculating these two fields. The next lemma helps us to further simplify this task.

Lemma 31. *We obtain a fundamental basis of the poloidal and toroidal fields on the sphere by choosing as the defining scalars Ψ, Φ the spherical harmonics multiplied by arbitrary functions that depend only on r:*

$$\Psi = f_{\ell m}(r)Y_{\ell m} \quad \textit{and} \quad \Phi = g_{\ell m}(r)Y_{\ell m}$$

So in order to determine F and G we expand their defining scalars in spherical harmonics in the usual manner and all we have to do is determine the coefficient functions. The time dependence is realized in the same way as in equations (3.18) to (3.20):

$$\Psi = \sum_{\ell=0}^{\infty} \sum_{m=-\ell}^{\ell} f_{\ell m}(r)Y_{\ell m}(\vartheta,\varphi)\mathrm{e}^{p_{\ell m}t}$$
$$\Phi = \sum_{\ell=0}^{\infty} \sum_{m=-\ell}^{\ell} g_{\ell m}(r)Y_{\ell m}(\vartheta,\varphi)\mathrm{e}^{p_{\ell m}t}$$

Again we drop the indices for better readability and with the calculations from above we see that the fields obtained in this way are given by

$$F = \begin{pmatrix} F_r \\ F_\vartheta \\ F_\varphi \end{pmatrix} = \nabla \times \Psi\mathbf{r} = \begin{pmatrix} 0 \\ \frac{f(r)}{r\sin\vartheta}\frac{\partial Y_{\ell m}}{\partial \varphi} \\ -\frac{f(r)}{r}\frac{\partial Y_{\ell m}}{\partial \vartheta} \end{pmatrix} \mathrm{e}^{p_{\ell m}t}$$
$$G = \begin{pmatrix} G_r \\ G_\vartheta \\ G_\varphi \end{pmatrix} = \nabla \times (\nabla \times \Phi\mathbf{r}) = \begin{pmatrix} \frac{\ell(\ell+1)}{r^2}g(r)Y_{\ell m} \\ \frac{1}{r}\frac{dg(r)}{dr}\frac{\partial Y_{\ell m}}{\partial \vartheta} \\ \frac{1}{r\sin\vartheta}\frac{dg(r)}{dr}\frac{\partial Y_{\ell m}}{\partial \varphi} \end{pmatrix} \mathrm{e}^{p_{\ell m}t}.$$

Now we can go about calculating f and g, the coefficients of the defining scalars for the toroidal and poloidal parts of the velocity field u. Since the radial component of the toroidal part is 0 only the poloidal part contributes to the radial velocity component which means

$$u_r = \frac{\ell(\ell+1)}{r^2}g(r)Y_{\ell m} \cdot \mathrm{e}^{p_{\ell m}t}$$

and using equation (3.19) we therefore find

$$\frac{W(r)}{r}Y_{\ell m} \cdot \mathrm{e}^{p_{\ell m}t} = \frac{\ell(\ell+1)}{r^2}g(r)Y_{\ell m} \cdot \mathrm{e}^{p_{\ell m}t}$$

which is equivalent to

$$g(r) = \frac{rW(r)}{\ell(\ell+1)}.$$

A similar calculation yields the relationship between f and Z: Since $u = F + G$ we have

$$\omega = \mathrm{curl}(u) = \mathrm{curl}(F+G) = \mathrm{curl}(F) + \mathrm{curl}(G).$$

Now curl(F) is a poloidal field with defining scalar Ψ and a rather lengthy but elementary calculation yields that curl(G) is a toroidal field with defining scalar $-\frac{1}{r^2}\Delta_{\vartheta,\varphi}\Phi - \frac{\partial^2\Phi}{\partial^2 r}$, so

$$\text{curl}(G))_r = 0$$

and therefore

$$\omega_r = (\text{curl}(F))_r = \frac{\ell(\ell+1)}{r^2} f(r) Y_{\ell m} \cdot \mathrm{e}^{p_{\ell m} t}.$$

Moreover, from equation (3.18) it follows that

$$\omega_r = \frac{Z(r)}{r} Y_{\ell m} \cdot \mathrm{e}^{p_{\ell m} t}$$

also holds and thus

$$f(r) = \frac{r Z(r)}{\ell(\ell+1)}.$$

By calculating the coefficients f and g we have now determined the scalar functions Φ and Ψ and therefore we can compute the complete velocity field u provided we can solve (3.21) to (3.23). This justifies the expansion in spherical harmonics and the consequent reduction to a system of ordinary differential equations.

3.3 A steady-state Bifurcation

Following [Chandrasekhar (1961)], Chapter VI, §57-§58, we now use our previous work of transforming the equations and expanding the solution in spherical harmonics to show that the onset of convection occurs through a steady state bifurcation. More precisely, we show that this is the case when the temperature gradient does not depend on the radius r explicitly and the same is the case for the gravitational field, which means $g(r)x \equiv gx$. As mentioned earlier the bifurcation parameter is the Rayleigh number C_ℓ. From our assumptions on the solution of the linearized system it is therefore clear that the bifurcation occurs when p crosses the imaginary axis for some ℓ,m which – since $\sigma = \frac{pR_2^2}{\nu}$ and $\nu, R_2 \in \mathbb{R}$ – happens if and only if σ crosses the i-axis. Saying that the bifurcation is steady-state (rather than Hopf) means we have to show that $\text{Im}(\sigma) = 0$ when the bifurcation occurs.

Throughout this section we focus on the case where $\beta_1 = 0$ and $\gamma = \gamma(r)$ is constant. From our earlier considerations we then deduce that

$$\beta = \beta_2 = \frac{\epsilon}{6\kappa} \quad \text{and} \quad \gamma = g\alpha.$$

This means that the temperature gradient is of the form $\nabla T = -2\beta\langle u,x\rangle$ with β independent of r. Equations (3.21) and (3.23) together then yield

$$\mathcal{D}_\ell(\mathcal{D}_\ell - \sigma)(\mathcal{D}_\ell - \mathcal{P}\sigma)W = -\ell(\ell+1)C_\ell W \tag{3.26}$$

where we define the Rayleigh number

$$C_\ell := \frac{2\beta\gamma}{\kappa\nu} R_2^6. \tag{3.27}$$

It is easy to check with Table 3.1 that C_ℓ is dimensionless. Because of the dependence on β it is proportional to the temperature gradient and therefore plays exactly the role we want it to. Before we show that the bifurcation is steady-state we take a closer look at properties of the operator $\mathcal{D}_\ell$ in the next lemma.

Lemma 32. *The operator $r^2\mathcal{D}_\ell$ is symmetric with respect to complex-valued L^2-functions f,g of r that vanish at the ends of an interval $[a,b]$, more precisely: For $f,g \in C^2([a,b])$ with $f(a) = f(b) = g(a) = g(b) = 0$ we have*

$$\int_a^b r^2 f \mathcal{D}_\ell g \mathrm{d}r = \int_a^b r^2 g \mathcal{D}_\ell f \mathrm{d}r.$$

Proof. Using the definition of $\mathcal{D}_\ell$ and integrating by parts twice we calculate

$$\begin{aligned}
\int_a^b r^2 f \mathcal{D}_\ell g \,\mathrm{d}r &= \int_a^b r^2 f \left\{ \frac{\mathrm{d}^2 g}{\mathrm{d}r^2} + \frac{2}{r}\frac{\mathrm{d}g}{\mathrm{d}r} - \frac{\ell(\ell+1)}{r^2} g \right\} \mathrm{d}r \\
&= \int_a^b \left\{ f \frac{\mathrm{d}}{\mathrm{d}r}\left(r^2 \frac{\mathrm{d}g}{\mathrm{d}r} \right) - \ell(\ell+1) f g \right\} \mathrm{d}r \\
&= r^2 f \frac{\mathrm{d}g}{\mathrm{d}r}\bigg|_a^b - \int_a^b \left\{ r^2 \frac{\mathrm{d}g}{\mathrm{d}r}\frac{\mathrm{d}f}{\mathrm{d}r} + \ell(\ell+1) f g \right\} \mathrm{d}r \\
&= r^2 \left(f \frac{\mathrm{d}g}{\mathrm{d}r} - g \frac{\mathrm{d}f}{\mathrm{d}r} \right)\bigg|_a^b + \int_a^b r^2 g \mathcal{D}_\ell f \,\mathrm{d}r \\
&= \int_a^b r^2 g \mathcal{D}_\ell f \,\mathrm{d}r.
\end{aligned}$$

□

Corollary 33. *It is worth noting that from the third row in the proof above we can immediately derive that for the complex-conjugate $\overline{f}$ of a function f we have*

$$\int_a^b r^2 f \mathcal{D}_\ell \overline{f} \,\mathrm{d}r = -\int_a^b \left\{ r^2 \left| \frac{\mathrm{d}f}{\mathrm{d}r} \right|^2 + \ell(\ell+1) |f|^2 \right\} \mathrm{d}r.$$

For a more compact notation in the following calculations let now

$$F(r) := \ell(\ell+1)\frac{\gamma}{\nu} R_2^4 \Theta(r)$$

and return to equations (3.21) to (3.23) which then take the form

$$\mathcal{D}_\ell(\mathcal{D}_\ell - \sigma)W = F \tag{3.28}$$

$$(\mathcal{D}_\ell - \sigma)Z = 0 \tag{3.29}$$

$$(\mathcal{D}_\ell - \mathcal{P}\sigma)F = -\ell(\ell+1)C_\ell W. \tag{3.30}$$

Transforming the boundary conditions (3.24) and (3.25) as well we get

$$W(\eta) = W(1) = F(\eta) = F(1) = 0 \quad \text{and} \quad \left.\frac{\mathrm{d}W}{\mathrm{d}r}\right|_{r=1,\eta} = 0. \tag{3.31}$$

Now we can formulate and prove the following proposition about the nature of the bifurcation that leads to the onset of convection.

Proposition 34. *The trivial equilibrium (pure heat conduction) loses its stability through a steady-state bifurcation, i.e., when σ crosses the imaginary axis then $\mathrm{Im}(\sigma) = 0$ and therefore $\sigma = 0$.*

Proof. We multiply (3.30) by $r^2\overline{F}$ and integrate over the interval $[\eta,1]$, the range of r. Note that because of (3.31) F vanishes at both ends of this interval and we can apply Corollary 33. We calculate

$$\begin{aligned}
&-\int_\eta^1 (\mathcal{D}_\ell - \mathcal{P}\sigma)F \cdot r^2\overline{F}\,\mathrm{d}r \\
&\quad= -\int_\eta^1 r^2\overline{F}\mathcal{D}_\ell F - \mathcal{P}\sigma r^2 F\overline{F}\,\mathrm{d}r \\
&\quad= \int_\eta^1 \left\{ r^2 \left|\frac{\mathrm{d}F}{\mathrm{d}r}\right|^2 + \ell(\ell+1)\left|F\right|^2 + \mathcal{P}\sigma r^2 \left|F\right|^2 \right\} \mathrm{d}r \\
&\quad= \ell(\ell+1)C_\ell \int_\eta^1 r^2 W\overline{F}\,\mathrm{d}r \\
&\quad= \ell(\ell+1)C_\ell \left[\int_\eta^1 r^2 W\mathcal{D}_\ell^2\overline{W}\,\mathrm{d}r - \overline{\sigma}\int_\eta^1 r^2 W\mathcal{D}_\ell\overline{W}\,\mathrm{d}r \right] \\
&\quad= \ell(\ell+1)C_\ell \left[-\left(r^2\frac{\mathrm{d}W}{\mathrm{d}r}\mathcal{D}_\ell\overline{W}\right)\Big|_\eta^1 + \int_\eta^1 r^2\left|\mathcal{D}_\ell W\right|^2\,\mathrm{d}r + \overline{\sigma}\int_\eta^1 r^2\left|\frac{\mathrm{d}W}{\mathrm{d}r}\right|^2 \right. \\
&\qquad\left. + \ell(\ell+1)\left|W\right|^2\,\mathrm{d}r \right] \\
&\quad= \ell(\ell+1)C_\ell \left[\int_\eta^1 r^2\left|\mathcal{D}_\ell W\right|^2\,\mathrm{d}r + \overline{\sigma}\int_\eta^1 r^2\left|\frac{\mathrm{d}W}{\mathrm{d}r}\right|^2 + \ell(\ell+1)\left|W\right|^2\,\mathrm{d}r \right]
\end{aligned}$$

where we used Corollary 33, equation (3.30), equation (3.28), integration by parts and the last boundary condition from (3.31) in this order. Combining the third and the last row of the calculation above we therefore obtain

$$\int_\eta^1 \left\{ r^2 \left| \frac{\mathrm{d}F}{\mathrm{d}r} \right|^2 + \ell(\ell+1)\left|F\right|^2 + \mathcal{P}\sigma r^2 \left|F\right|^2 \right\} \mathrm{d}r$$
$$- \ell(\ell+1)C_\ell \left[\int_\eta^1 r^2 \left|\mathcal{D}_\ell W\right|^2 \, \mathrm{d}r + \overline{\sigma} \int_\eta^1 r^2 \left| \frac{\mathrm{d}W}{\mathrm{d}r} \right|^2 + \ell(\ell+1)\left|W\right|^2 \, \mathrm{d}r \right] = 0.$$

Both the real and the imaginary part of the left hand side have to be zero. Note that except for σ all quantities in the equation are real. The vanishing of the imaginary part gives

$$\mathrm{Im}(\sigma) \left\{ \mathcal{P} \int_\eta^1 r^2 \left|F\right|^2 \, \mathrm{d}r + \ell(\ell+1)C_\ell \int_\eta^1 r^2 \left| \frac{\mathrm{d}W}{\mathrm{d}r} \right|^2 + \ell(\ell+1)\left|W\right|^2 \, \mathrm{d}r \right\} = 0.$$

The factor inside the curly brackets is positive, so this yields $\mathrm{Im}(\sigma) = 0$, which means there is a zero eigenvalue and thus the bifurcation is steady-state. □

The Critical Eigenspaces

Now we are in a position to investigate the nature of the critical eigenspaces corresponding to the eigenvalues that cross the i-axis. We set $\sigma = 0$ in equations (3.28) to (3.30). By doing so we obtain the following equations that govern the problem at the bifurcation point:

$$\mathcal{D}_\ell Z = 0 \tag{3.32}$$
$$\mathcal{D}_\ell^2 W = F \tag{3.33}$$
$$\mathcal{D}_\ell F = -\ell(\ell+1)C_\ell W \tag{3.34}$$

The boundary conditions of course remain the same, cf. (3.31). Equation (3.32) demands that $Z \equiv 0$, so the radial component of the vorticity vanishes. The velocity field is therefore purely poloidal.

Equations (3.33) and (3.34) reduce to an eigenvalue problem for the operator $-\mathcal{D}_\ell^3$,

$$-\mathcal{D}_\ell^3 W(r) = \ell(\ell+1)C_\ell W(r), \tag{3.35}$$

with boundary conditions

$$W(\eta) = W(1) = 0, \quad \left.\frac{\mathrm{d}W}{\mathrm{d}r}\right|_{r=1,\eta} = 0 \quad \text{and} \quad \left.\mathcal{D}_\ell^2 W\right|_{r=1,\eta} = 0, \tag{3.36}$$

where the last condition follows from (3.33) and $F(\eta) = F(1) = 0$. Each non-trivial solution of (3.35) with boundary conditions (3.36) is associated with a characteristic value for $-\mathcal{D}_\ell^3$

and thus with a Rayleigh number C_ℓ. We are interested in the lowest such C_ℓ and therefore in the lowest characteristic value of $-\mathcal{D}_\ell^3$. In this situation the following lemma comes in handy.

Lemma 35. *The operator $-\mathcal{D}_\ell^3$ has positive and simple characteristic values. If for fixed ℓ we denote by $\Lambda_{1\ell}$ the smallest of these values and by $C_{1\ell}$ the associated Rayleigh number then the following is true:*

$$C_{1\ell} \overset{\ell\to\infty}{\longrightarrow} \infty$$

This lemma and a sketch of its proof can be found in [Chossat (1979)]. We outline part of a similar proof regarding the statement on simplicity and positivity of the eigenvalues in the next section. It immediately follows now that there exists a lowest integer value ℓ_0 such that C_{ℓ_0} is the smallest characteristic value, minimizing over ℓ now. This is the critical Rayleigh number, for which instability sets in. The associated space V_{ℓ_0} is the first to lose stability and the spherical harmonics of degree ℓ_0 determine the form of the first convective flow patterns.

3.4 Secondary Bifurcations and Mode Interaction

Up to now we have assumed the radius ratio η of the two spheres to be a fixed value. Now we want to investigate the influence of η as a secondary bifurcation parameter on the value $\ell_0 = \ell_0(\eta)$, the index of the first mode to go unstable, as defined above. In fact, it turns out that ℓ_0 tends to infinity when η is taken arbitrarily close to 1 which was proved in [Chossat (1979)] as Lemma 6. We reproduce the proof in detail below. This result gives rise to a phenomenon that is called **mode interaction** referring to the dynamical behavior of the system at parameter values for which several eigenspaces become unstable simultaneously. As we will see later these cases exhibit particularly interesting dynamics such as heteroclinic connections between equilibria.

Proposition 36. $\ell_0(\eta) \to \infty$ *when* $\eta \to 1$.

Proof. We use the same notation as in Lemma 35. In order to prove our claim we actually show that the following is true:

$$\forall k\in\mathbb{N} \quad \exists V(1)\colon\ \forall \eta \in V(1)\colon \quad \left[\ell(\ell+1) \le \frac{k}{2}(k+1)\right] \Rightarrow C_{1k} < C_{1\ell} \tag{3.37}$$

Here $V(1)$ is a neighborhood of 1. To see that (3.37) indeed implies the desired statement note that the left inequality definitely holds for all $\ell < \frac{k}{2}$. So if we can prove the implication this means that for any $k \in \mathbb{N}$ and η close enough to 1 we have $C_{1k} < C_{1\ell}$ for those values of ℓ. Therefore the lowest $C_{1\ell}$ is definitely not attained for $\ell < \frac{k}{2}$ which means that $\ell_0(\eta) \ge \frac{k}{2}$ for all $\eta \in V(1)$, so $\ell_0 \overset{\eta\to 1}{\longrightarrow} \infty$ because k was arbitrary. Thus (3.37) is really all we need to prove.

Now let us begin to prove (3.37) by performing the following change of variable

$$s := \frac{r}{1-\eta} + \frac{1-2\eta}{1-\eta} = \frac{r+1-2\eta}{1-\eta}, \quad r \in [\eta,1]$$

after which we have $s \in [1,2]$. Because of

$$\frac{\mathrm{d}r(s)}{\mathrm{d}s} = 1-\eta$$

we calculate for $W = W(r(s))$

$$\begin{aligned}
\mathcal{D}_\ell W &= \left[\frac{\mathrm{d}^2}{\mathrm{d}r^2} + \frac{2}{r}\frac{\mathrm{d}}{\mathrm{d}r} - \frac{\ell(\ell+1)}{r^2}\right] W \\
&= \frac{1}{(1-\eta)^2}\left[(1-\eta)^2\frac{\mathrm{d}^2}{\mathrm{d}r^2} + \frac{2(1-\eta)^2}{r}\frac{\mathrm{d}}{\mathrm{d}r} - \frac{\ell(\ell+1)(1-\eta)^2}{r^2}\right] W \\
&= \frac{1}{(1-\eta)^2}\underbrace{\left[\frac{\mathrm{d}^2}{\mathrm{d}s^2} + \frac{2(1-\eta)}{(1-\eta)s+2\eta-1}\frac{\mathrm{d}}{\mathrm{d}s} - \frac{\ell(\ell+1)(1-\eta)^2}{[(1-\eta)s+2\eta-1]^2}\right]}_{=:\widetilde{\mathcal{D}}_{\ell,\eta}} W.
\end{aligned}$$

This transforms equation (3.35) into

$$-\widetilde{\mathcal{D}}^3_{\ell,\eta} W = (1-\eta)^6 \ell(\ell+1) C_\ell W. \tag{3.38}$$

The boundary conditions (for $s = 1,2$ now) remain homogeneous. It is clear that

$$\widetilde{\mathcal{D}}_{\ell,\eta} \longrightarrow \frac{\mathrm{d}^2}{\mathrm{d}s^2} \quad \text{uniformly as} \quad \eta \to 1$$

and therefore

$$-\widetilde{\mathcal{D}}^3_{\ell,\eta} \longrightarrow -\frac{\mathrm{d}^6}{\mathrm{d}s^6} \quad \text{uniformly as} \quad \eta \to 1.$$

This is important since we want to deduce that the eigenvalues of the operator $-\widetilde{\mathcal{D}}^3_{\ell,\eta}$ with homogeneous boundary conditions (3.36) are positive and simple. We only sketch the proof of this here: Because of the above it suffices to show that the eigenvalues of $-\frac{\mathrm{d}^6}{\mathrm{d}s^6}$ (with analogous homogeneous boundary conditions) are positive and simple. This follows from a result on integral equations with oscillation kernels in [Joseph (1976)], Appendix D. In fact what is shown there is that the eigenvalues of an integral equation

$$\phi(x) = \lambda \int_a^b K(x,s)\phi(s)\,\mathrm{d}\sigma(s)$$

are positive and simple if $K(x,s)$ is an oscillation kernel, a term that is also defined in Appendix D of [Joseph (1976)]. Thus we convert our eigenvalue problem into an integral equation by turning to the Green function and the question then becomes whether or not the

Green function is oscillatory. Furthermore, it is shown in [Joseph (1976)] that (under certain additional assumptions) for a differential operator L that can be written in the form

$$L(u) = \mu_0(x)\frac{\mathrm{d}}{\mathrm{d}x}\mu_1(x)\frac{\mathrm{d}}{\mathrm{d}x}\cdots\frac{\mathrm{d}}{\mathrm{d}x}\mu_n(x)u \tag{3.39}$$

the corresponding Green function is in fact oscillatory. Note that a bit of caution is required regarding $\pm$-signs here. Then the theorem mentioned above yields that all the eigenvalues of L are positive and simple. Clearly the operator $-\frac{\mathrm{d}^6}{\mathrm{d}s^6}$ is of the iterated form (3.39). Thus this line of reasoning applies and $-\frac{\mathrm{d}^6}{\mathrm{d}s^6}$ has only positive and simple eigenvalues and so does $-\widetilde{\mathcal{D}}^3_{\ell,\eta}$.

Denote now by $\Lambda_{1\ell}(\eta)$ the smallest of the eigenvalues of $-\widetilde{\mathcal{D}}^3_{\ell,\eta}$ and by Λ_1 the smallest eigenvalue of $-\frac{\mathrm{d}^6}{\mathrm{d}s^6}$. Then we have

$$\Lambda_{1\ell}(\eta) \xrightarrow{\eta\to 1} \Lambda_1$$

uniformly for bounded ℓ. This implies that for any fixed $k \in \mathbb{N}$ there is a neighborhood $V(1)$ such that for $\eta \in V(1)$ and $0 \le \ell < k$ we get

$$\Lambda_{1k}(\eta) < 2\Lambda_{1\ell}(\eta).$$

Now these eigenvalues are of the form given in (3.38) and substitution yields

$$\ell < k \quad \Rightarrow \quad k(k+1)C_{1k} < 2\ell(\ell+1)C_{1\ell}.$$

Therefore we have

$$\left[\ell(\ell+1) \le \frac{k}{2}(k+1)\right] \quad \Rightarrow \quad C_{1k} < C_{1\ell}$$

for all $\eta \in V(1)$ which completes the proof. □

We now want to look more closely at particularly interesting parameter situations that we call **mode interactions**. In order to put things into proper perspective let us go back a little bit: It is our general aim to investigate local bifurcations in the spherical Bénard problem, i.e., changes in the stability properties of equilibria, periodic orbits or other invariant sets. The classical approach is to look at a parameter-dependent equilibrium $x_0(\lambda)$ and determine a parameter value λ_0 for which new solutions appear close to x_0. We then say that a solution branch bifurcates from $x_0(\lambda)$ at λ_0. There are two principal ways in which this can happen that can be distinguished by the nature of the critical eigenvalues of the Jacobian, more precisely by the imaginary part of the eigenvalue crossing the imaginary axis as the bifurcation parameter reaches its critical value λ_0:

- a steady state bifurcation, corresponding to a zero eigenvalue
- a Hopf bifurcation, corresponding to a pair of purely imaginary eigenvalues

These two cases display qualitatively different dynamical behavior: The first is called steady-state because the new solutions branching off of $x_0(\lambda)$ are equilibria themselves whereas in the second case the new solution is a periodic orbit. Of course, in a system of sufficiently high dimension two local bifurcations can occur at the same time, or more precisely for the same critical parameter value λ_0. The eigenspaces of the critical eigenvalues are often called **modes** and this phenomenon is referred to as **mode interaction**. The simultaneous onset of instability for two different modes often leads to complex (and therefore interesting) dynamics, the modes are **interacting**. Due to the above classification there are three types of mode interaction: steady-state/steady-state, steady-state/Hopf and Hopf/Hopf.

As we saw in section 3.1 for the spherical Bénard problem the modes are just the spaces V_ℓ of spherical harmonics of degree $\ell \in \mathbb{N}$. Generically they lose their stability one at a time. We showed in Proposition 34 that under certain assumptions the bifurcation that causes the onset of convection is a steady-state bifurcation.

Furthermore, we proved above that the value of ℓ of the first unstable mode V_ℓ tends to infinity as the secondary bifurcation parameter, η, the ratio of the radii of the two shells, is taken closer to 1. Since ℓ is a natural number this implies that there must be certain values η_0 for which the critical modes of degree ℓ and $\ell + 1$ go unstable at the same Rayleigh number. Qualitatively an η-ℓ_0-diagram looks like Figure 3.2. For such a parameter value η_0 a mode interaction occurs. Under the assumptions from above it is a steady-state/steady-state interaction.

In the simplest of these cases we have $\ell = 1$. It is usually referred to as the 1-2 mode interaction and has been studied by many different authors, such as [Armbruster and Chossat (1991)] and [Friedrich and Haken (1986)] to mention just two. In the 1-2 mode interac-

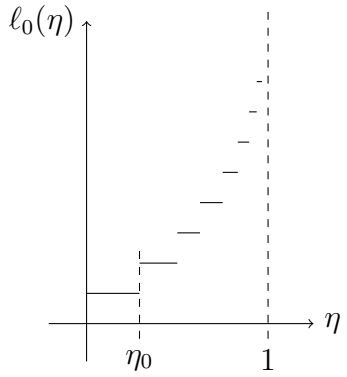

Figure 3.2: Index of the most unstable mode

tion we have V_1 and V_2 going unstable simultaneously. The critical eigenspace is therefore $V := V_1 \oplus V_2$. Note that $\dim(V_\ell) = 2\ell + 1$ so $\dim(V) = 3 + 5 = 8$. We introduce coordinates on this space in the following manner: Let X be the projection of the original state variable onto V. In V_1 denote by x_i the coordinate of X in the direction of the eigenvec-

tor corresponding to the spherical harmonic Y_{1i}, $i \in \{0, \pm 1\}$, and accordingly on V_2 with $y_j, j \in \{0, \pm 1, \pm 2\}$, for the eigendirections corresponding to Y_{2j}. We write $\mathbf{x} = (x_{-1},x_0,x_1)$ and $\mathbf{y} = (y_{-2},y_{-1},y_0,y_1,y_2)$ and therefore an element of V is generally of the form $(\mathbf{x},\mathbf{y})$ with $\mathbf{x} \in V_1, \mathbf{y} \in V_2$.

To simplify the local stability analysis it is suitable to perform a center manifold reduction of the system. Note that it is now crucial that we can do this in an infinite dimensional setting. The center manifold is eight-dimensional and tangent to V at the bifurcation point. [Chossat et al. (1999)] state that according to the results of section 2.4 we obtain a reduced system of the form

$$\frac{\mathrm{d}X}{\mathrm{d}t} = F(X,\lambda_1,\lambda_2) \tag{3.40}$$

where λ_1 and λ_2 are suitable linear combinations of the deviations from the critical values of the ratio of the radii η and the Rayleigh number C_ℓ, respectively. In the following we therefore consider λ_2 as the primary bifurcation parameter and λ_1 as the secondary one, just like before. Without loss of generality we assume the critical values of both parameters to be 0. We now face the task of determining F, i.e., calculating its Taylor expansion up to some finite order. We know from section 2.2 that there exist finite sets of invariant polynomials and equivariant mappings that generate the ring $\mathcal{P}(O(3))$ and the module $\vec{\mathcal{P}}(O(3))$, respectively. These have been computed by [Chossat et al. (1999)]. In fact, what is shown there is that

- the $O(3)$-invariant polynomials $V \to \mathbb{R}$ are generated by five linearly independent polynomials, let us denote them by $\pi_1,...,\pi_5$,
- there are three linearly independent $O(3)$-equivariant mappings $\Sigma_1, \Sigma_2, \Sigma_3 : V_1 \to V_1$ and five linearly independent $O(3)$-equivariant mappings $\Upsilon_1,...,\Upsilon_5 : V_2 \to V_2$, so that $\vec{\mathcal{P}}(O(3))$ is generated by eight mappings of the form $(\Sigma_i,0)$ and $(0,\Upsilon_j)$.

Let us take a closer look at and exploit the symmetry of our system. Bearing in mind that we would like to apply the equivariant branching lemma we have to determine the isotropy lattice of the natural representation of $O(3)$ on $V_1 \oplus V_2$. This is done in Appendix A of [Armbruster and Chossat (1991)] and in [Chossat et al. (1999)] we find the partially ordered set depicted in Figure 3.3.

The entries in curly brackets denote the coordinates of the fixed-point space associated with a representative of the corresponding isotropy type. Recall from before that $\mathbb{Z}_2^c = \{\pm \mathbb{1}\}$ where $-\mathbb{1}$ is the reflexion through the origin in $\mathbb{R}^3$. Therefore $O(2) \oplus \mathbb{Z}_2^c$ is the group of all motions of an (infinite) cylinder that preserve the origin. $\mathbb{Z}_2^-$ is another manifestation of $\mathbb{Z}_2$ that is not conjugate to $\mathbb{Z}_2^c$. It is generated by a reflexion across a plane in $\mathbb{R}^3$. Such a reflexion is equivalent to the composition of a rotation of angle π around an axis composed with a reflexion through the origin, hence the terminology with the minus sign that is reminiscent of the reflexion through the origin. For the other groups superscripts are used in the same way to distinguish non-conjugate manifestations. By $\mathbb{D}_n$ we denote the dihedral group of

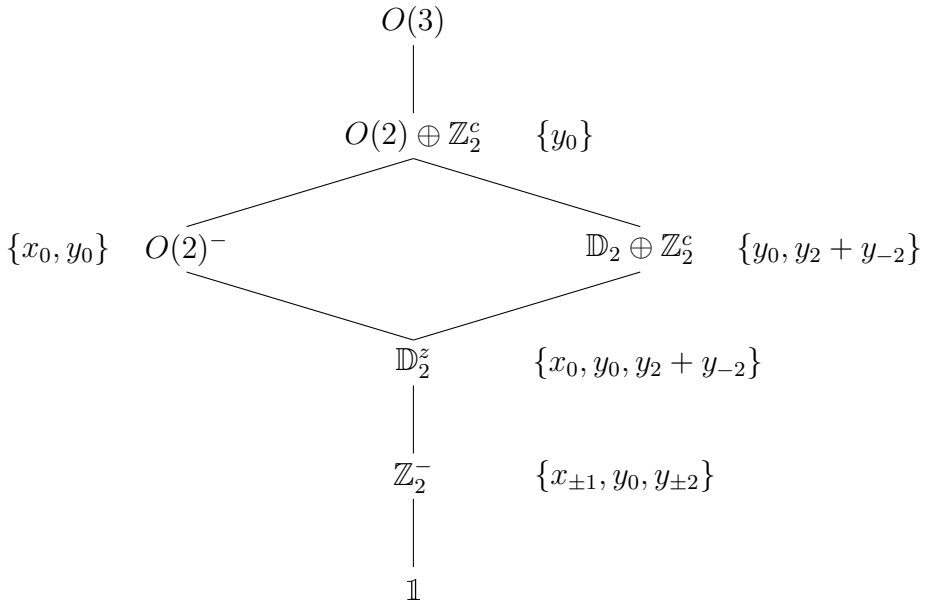

Figure 3.3: The Isotropy Lattice

order $2n$, the symmetry group of a regular n-gon. Finally $O(2)^-$ is the symmetry group of the double cone. For a more detailed discussion of the isotropy lattice see [Armbruster and Chossat (1991)].

According to [Chossat et al. (1999)] the expansion up to third order of the right hand side of equation (3.40) takes the form

$$\begin{cases} \dot{x}_j &= x_j(\lambda_1 + \gamma\pi_1 + \delta\pi_2) + \beta\Sigma_j^2(\mathbf{x},\mathbf{y}) + \delta'\Sigma_j^3(\mathbf{x},\mathbf{y},\mathbf{y}) \\ \dot{y}_m &= y_m(\lambda_2 + d\pi_1 + f\pi_2) + b\Upsilon_m^2(\mathbf{x},\mathbf{x}) + c\Upsilon_m^3(\mathbf{y},\mathbf{y}) + f'\Upsilon_m^4(\mathbf{x},\mathbf{x},\mathbf{y}). \end{cases} \tag{3.41}$$

We do not go into details on all the coefficients in these equations. In the following section we look for heteroclinic cycles and only make more precise what is important for our purposes. A detailed description and a guideline to the derivation can be found in [Chossat et al. (1999)].

3.5 Existence of Heteroclinic Cycles

In this section we use our previous results to investigate the system with respect to heteroclinic cycles, i.e., collections of trajectories that connect different equilibria in a way that is made precise below. As we will see the existence of such cycles is closely related to the symmetry of the system. In general they do not exist in systems without symmetry which follows from a well-known theorem on structural stability that we state below. Heteroclinic cycles play a role in the explanation of phenomena such as the aperiodic reversals of the polarity which the Earth's magnetic field exhibits, see section 4.1 for geophysical informa-

tion on this. The following definition and considerations are inspired by [Melbourne et al. (1989)].

Definition 37. Let S_1,...,S_{k+1} be flow-invariant sets for a system of Γ-equivariant differential equations and let S_{k+1} be a conjugate of S_1. We call a set of trajectories $x_1(t), \ldots, x_k(t)$ a **heteroclinic cycle** if x_j connects S_j with S_{j+1} in the sense that we have $x_j(t) \to S_{j+1}$ for $t \to \infty$ and $x_j(t) \to S_j$ for $t \to -\infty$.

In order to see why such connections are not structurally stable consider the following theorem from [Palis and de Melo (1982)], page 127.

Theorem 38. *An r-times continuously differentiable vector field X on a smooth manifold M is structurally stable (in the sense that there is a neighborhood in which all other vector fields are topologically equivalent) if it satisfies the following properties:*

- *There are finitely many critical elements, i.e., equilibria and periodic orbits, all of which are hyperbolic.*
- *For two critical elements their stable and unstable manifolds intersect transversally.*
- *The set of non-wandering points is equal to the union of the critical elements.*

The crucial point for the structural instability of vector fields with heteroclinic cycles is the second property. Suppose we have a system with a heteroclinic cycle that connects two equilibria. Then both of these are saddles, of course, and the intersection of their stable and unstable manifold is just the trajectory connecting the two. In a point on that trajectory the tangent space on both manifolds contains the direction tangent to the trajectory and therefore the intersection is certainly not transversal. So vector fields with heteroclinic cycles are not structurally stable.

In a system with symmetry, however, it is not unreasonable to expect heteroclinic cycles and they can actually be structurally stable if we consider only equivariant perturbations. To see why this is the case recall from Proposition 7 that the fixed-point space of an isotropy subgroup is flow-invariant under the equivariant mapping. Suppose now we have two non-trivial equilibria α and β and two isotropy subgroups Σ_1, Σ_2 such that

- $\alpha, \beta \in \text{Fix}(\Sigma_1) \cap \text{Fix}(\Sigma_2)$,
- $\dim(\text{Fix}(\Sigma_1)) = \dim(\text{Fix}(\Sigma_2)) = 2$,
- $\text{Fix}(\Sigma_1) \neq \text{Fix}(\Sigma_2)$.

Moreover, suppose that α and β are saddles that have bifurcated from the trivial equilibrium 0. Now in $\text{Fix}(\Sigma_1)$ let α be sink, β a saddle and let the unstable manifold of β coincide with the stable manifold of α and conversely in $\text{Fix}(\Sigma_2)$. Then there exists a heteroclinic cycle connecting α and β in the three-dimensional space $\text{span}(\text{Fix}(\Sigma_1) \cup \text{Fix}(\Sigma_2))$, cf. Figure 3.4.

Note that equivariant perturbations preserve the invariance of the fixed-point spaces. Within $\mathrm{Fix}(\Sigma_i)$ we have saddle-sink connections and those are stable in $\mathbb{R}^2$, in contrast to saddle-saddle connections, as indicated above. Thus the heteroclinic cycle is structurally stable in the sense that symmetry preserving perturbations do not destroy it. Of course one can easily imagine a more complex heteroclinic cycle involving more than two equilibria or periodic orbits. Now we investigate the isotropy lattice for the Bénard problem aiming to discover similar structures there. We explain how the simplest heteroclinic cycle for the 1-2 mode interaction can be found.

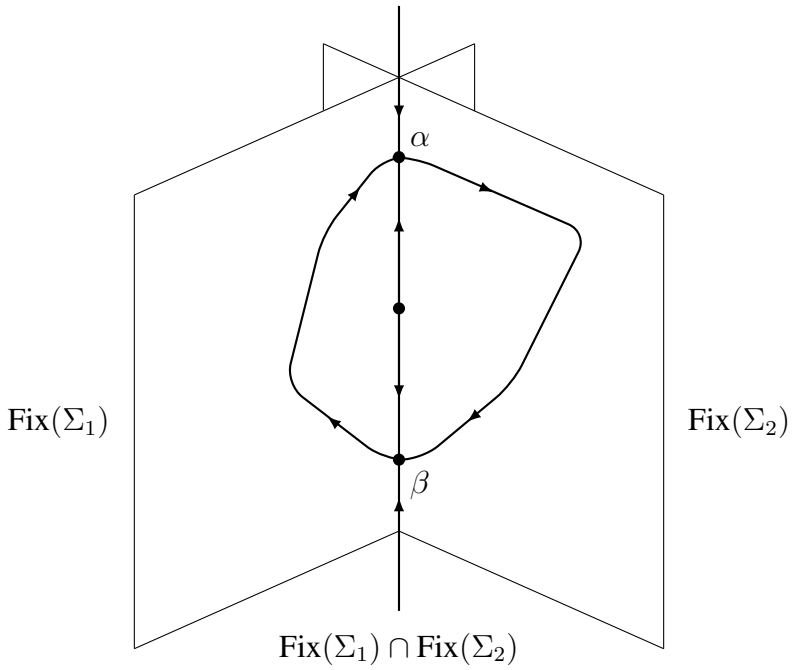

Figure 3.4: A simple heteroclinic cycle

Phase Portrait in $\mathbf{L} := \mathbf{Fix}(\mathbf{O(2)} \oplus \mathbb{Z}_\mathbf{2}^\mathbf{c})$

Clearly, there is only one maximal isotropy subgroup in the isotropy lattice for the spherical Bénard problem, namely $O(2) \oplus \mathbb{Z}_2^c$. If we restrict system (3.41) to $L = \mathrm{span}\{y_0\}$ the conditions of the equivariant branching lemma are satisfied, so there exists a unique branch of solutions with symmetry group $O(2) \oplus \mathbb{Z}_2^c$ emanating from the trivial solution. In accordance with [Chossat et al. (1999)] we choose $f = -1$ and the equation then reads

$$\dot{y}_0 = y_0(\lambda_2 + cy_0 - y_0^2).$$

Therefore we have to investigate

$$0 = y_0(\lambda_2 + cy_0 - y_0^2). \tag{3.42}$$

Let us now discuss what happens here: If $c = 0$ equation (3.42) takes the form

$$y_0\lambda_2 - y_0^3 = 0 \tag{3.43}$$

which is precisely the normal form of the pitchfork bifurcation. There are two bifurcating solution branches corresponding to $y_0 = \pm\sqrt{\lambda_2}$ and the bifurcation diagram looks like Figure 3.5 (a).

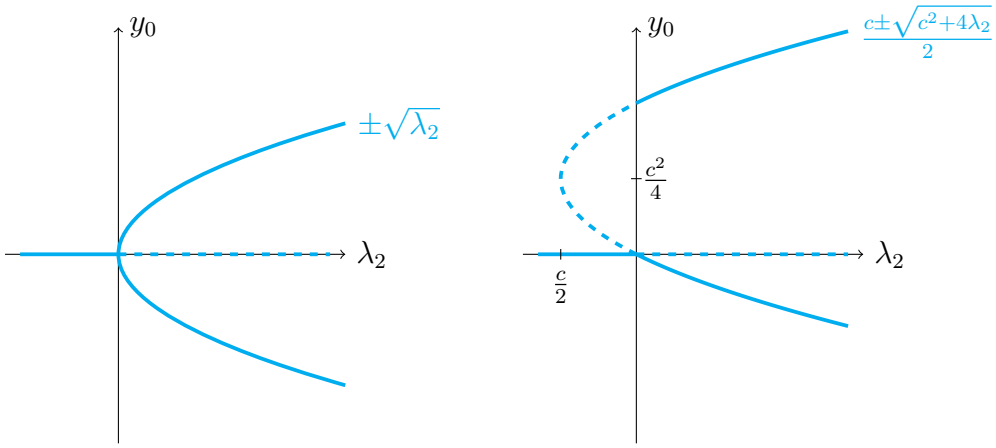

(a) $c = 0$ **(b)** $|c|$ *small*

Figure 3.5: Bifurcation Diagrams for L

If we take c to be different from 0 but $|c| \ll 1$ the bifurcation is transcritical as shown in Figure 3.5 (b). Since one of the branches contains a turning point close to 0 there are again two new solution branches for $\lambda_2 > 0$, now corresponding to $y_0 = {}^1\!/_2(c \pm \sqrt{c^2 + 4\lambda_2})$. According to [Chossat et al. (1999)] it is reasonable to assume c to be such a small parameter for the Bénard problem. Thus in any case we have two bifurcating non-trivial equilibria in L that are both stable after the trivial solution loses its stability. Let us call them α and β, respectively. The dynamics in L for $\lambda_2 > 0$ are depicted in Figure 3.6.

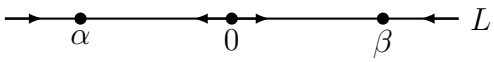

Figure 3.6: Dynamics in L

Phase Portrait in $\mathbf{P_1} := \mathbf{Fix}(\mathbb{D}_\mathbf{2} \oplus \mathbb{Z}_\mathbf{2}^\mathbf{c})$

This fixed-point space is two-dimensional and contains L, in particular we have $\mathbf{x} = 0$ here and therefore pure $\ell = 2$ mode dynamics. Earlier we chose $f < 0$ which according to [Armbruster and Chossat (1991)] ensures the stability of either α or β in P_1. Apart from the axis L the plane P_1 contains two more one-dimensional invariant subspaces L' and L'' which are conjugates of L by rotations of angle ${}^{2\pi}\!/_3$ and ${}^{4\pi}\!/_3$, respectively. There are also conjugates of the equilibria α and β in L' and L'', let us call them α', α'' and β', β''. Conjugate equilibria of course have the same stability properties. Thus (for $c < 0$) the phase portrait in P_1 looks like Figure 3.7. Changing the sign of c only leads to a reversal of the arrows in the diagram.

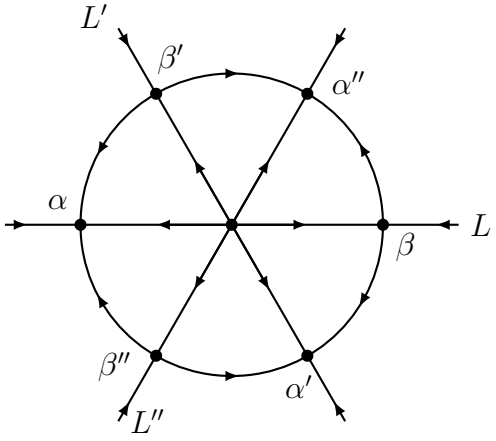

Figure 3.7: Dynamics in P_1, $\lambda_2 > 0, f < 0, c < 0$

Phase Portrait in $\mathbf{P_2} := \mathbf{Fix}(\mathbf{O(2)}^-)$

From system (3.41) we deduce that the analysis of the dynamics in this plane reduces to the study of

$$\begin{cases} \dot{x}_0 = x_0(\lambda_1 + \gamma x_0^2 + \beta y_0 + (\delta + \frac{3}{2}\delta')y_0^2) \\ \dot{y}_0 = y_0(\lambda_2 + cy_0 - y_0^2) + x_0^2(1 + (d - f')y_0) \end{cases} . \tag{3.44}$$

[Armbruster and Chossat (1991)] argue that it is of physical relevance to consider $\gamma < 0$ and suitable rescaling enables us to set $\beta = -1$. We investigate the further simplification $\delta = \delta' = c = 0$, so the equations looks like

$$\begin{cases} \dot{x}_0 = x_0(\lambda_1 + \gamma x_0^2 - y_0) \\ \dot{y}_0 = y_0(\lambda_2 - y_0^2) + x_0^2(1 + (d - f')y_0) \end{cases} . \tag{3.45}$$

If we linearize the right hand side at the equilibrium $\alpha = (0, -\sqrt{\lambda_2})$ we get

$$\begin{aligned} L|_\alpha &= \begin{pmatrix} \lambda_1 + 3\gamma x_0^2 - y_0 & -x_0 \\ 2x_0(1 + (d - f')y_0) & \lambda_2 - 3y_0^2 + (d - f')x_0^2 \end{pmatrix}\Bigg|_\alpha \\ &= \begin{pmatrix} \lambda_1 + \sqrt{\lambda_2} & 0 \\ 0 & -2\lambda_2 \end{pmatrix}. \end{aligned} \tag{3.46}$$

For the linearization in $\beta = (0, \sqrt{\lambda_2})$ we obtain

$$L|_\beta = \begin{pmatrix} \lambda_1 - \sqrt{\lambda_2} & 0 \\ 0 & -2\lambda_2 \end{pmatrix}. \tag{3.47}$$

We fix λ_2 and let λ_1 vary from $-\infty$ to positive values. Obviously the eigenvalue $-2\lambda_2^2$ is always negative, this corresponds to the stable directions of α and β along L. For $L|_\alpha$

the other eigenvalue $\lambda_1 + \sqrt{\lambda_2}$ is negative for very negative λ_1 but changes its sign when $\lambda_1 = -\sqrt{\lambda_2}$. This is where we can look for new equilibria that bifurcate from α. In order to do so we solve

$$\begin{cases} 0 = \dot{x}_0 = x_0(\lambda_1 + \gamma x_0^2 - y_0) \\ 0 = \dot{y}_0 = y_0(\lambda_2 - y_0^2) + x_0^2(1 + (d - f')y_0) \end{cases} \tag{3.48}$$

with the restriction that $x_0 \neq 0$ and therefore $y_0 = \lambda_1 + \gamma x_0^2$ from the first equation. Substituting this into the second equation of (3.48) we get

$$\begin{aligned} 0 &= y_0(\lambda_2 - y_0^2) + x_0^2(1 + (f - f')y_0) \\ &= (\lambda_1 + \gamma x_0^2)(\lambda_2 - (\lambda_1 + \gamma x_0^2)^2) + x_0^2(1 + (f - f')(\lambda_1 + \gamma x_0^2)). \end{aligned}$$

Let us write $a := x_0^2$ and call the right hand side $p = p(a,\lambda_1)$. Then p is a polynomial of third degree in a with leading coefficient $-\gamma^3 > 0$ and $p(0,\lambda_1) = \lambda_1\lambda_2 - \lambda_1^3$. Since $a = x_0^2$ there are new solutions $x := \pm\sqrt{\tilde{a}}$ if $p(\tilde{a}) = 0$ for some $\tilde{a} > 0$. Such an $\tilde{a}$ certainly exists for parameter values λ_1 where $p(0,\lambda_1) < 0$. We have

$$p(0,\lambda_1) = 0 \quad \Leftrightarrow \quad \lambda_1 = 0 \ \vee \ \lambda_1 = \pm\sqrt{\lambda_2}$$

and therefore $p(0,\lambda_1) < 0$ for $\lambda_1 \in (-\sqrt{\lambda_2},0)$ and for $\lambda_1 > \sqrt{\lambda_2}$. So indeed there is a new branch of solutions bifurcating from α when $\lambda_1 = -\sqrt{\lambda_2}$. We call these new equilibria **type 2 solutions**. The branch ceases to exist when $\lambda_1 = 0$. From (3.47) it is clear that at $\lambda_1 = \sqrt{\lambda_2}$ the other equilibrium, β, loses its stability and another branch of new equilibria bifurcates from β.

A more detailed bifurcation analysis is rather cumbersome to do by hand and can best be performed with a path-following algorithm such as AUTO, cf. [Doedel and Oldeman (2009)]. We list the results obtained by [Armbruster and Chossat (1991)] in this way. Note that there are no qualitative changes if we loosen the restrictions on the parameter values from above, particularly if $c \neq 0$, $|c| \ll 1$.

- At $\lambda_1 = -\frac{1}{2}\sqrt{3\lambda_2}$ a Hopf bifurcation occurs where the type 2 solutions lose their stability and a stable periodic orbit appears.
- At $\lambda_1 = -\frac{1}{2}\sqrt{\lambda_2}$ the periodic orbit meets the stable manifold of the origin and disappears.

The heteroclinic cycle

We now combine these results to discover a heteroclinic cycle in the three-dimensional space that is spanned by the two planes P_1 and P_2. For $\lambda_2 > 0$ there is a connection from β to α in P_1 and accordingly for their conjugates as we saw above. So all we need to complete a heteroclinic cycle is a connection from α to β, β' or β''. Such a connection can be found

in P_2 as we visualize in Figure 3.8: The first type 2 equilibrium γ_1 bifurcates from α at $\lambda_1 = -\sqrt{\lambda_2}$ and undergoes a Hopf bifurcation where it loses its stability. The stable periodic orbit that is born meets the stable manifold of the origin at $\lambda_1 = -\frac{1}{2}\sqrt{\lambda_2}$ as seen in Figure 3.8 (d). A connection is then established from α to β as in Figure 3.8 (e). At $\lambda_1 = 0$ the origin loses its stable direction and becomes a source while the $\alpha - \beta$ connection persists, Figure 3.8 (f). When the new type 2 solutions γ_2 branch off of β at $\lambda_1 = \sqrt{\lambda_2}$ the heteroclinic connection ceases to exist since β turns into a saddle and the unstable manifold of α then connects to γ_2. Therefore we have an $\alpha - \beta$ connection in P_2 and thus a heteroclinic cycle in $P_1 \oplus P_2$ for

$$\lambda_1 \in \left(-\tfrac{1}{2}\sqrt{\lambda_2}, \sqrt{\lambda_2}\right).$$

Note the resemblance to the theoretically constructed cycle in Figure 3.4.

A further investigation shows that more heteroclinic cycles can be discovered in this setting, which exhibit different structures and involve other equilibria. It is also interesting to discuss stability and attraction of these cycles. Figures 3.7 and 3.8 suggest that the cycle from above is locally attracting since trajectories in a neighborhood have "nowhere else to go". At least this holds in the three-dimensional subspace $P_1 \oplus P_2$. For a more detailed discussion of heteroclinic cycles in the Bénard problem we refer the reader to [Chossat et al. (1999)] and [Armbruster and Chossat (1991)].

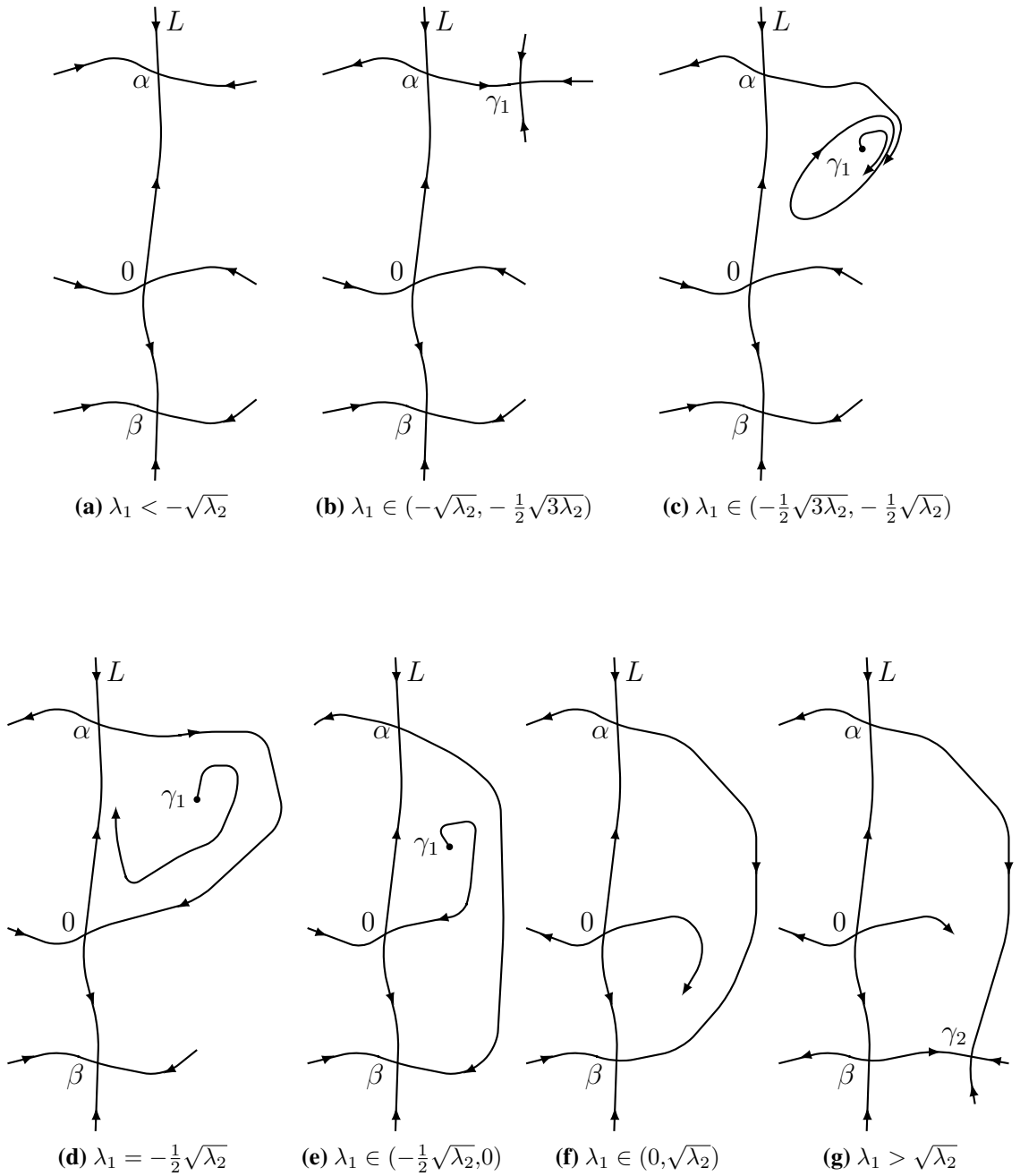

(a) $\lambda_1 < -\sqrt{\lambda_2}$ **(b)** $\lambda_1 \in (-\sqrt{\lambda_2}, -\frac{1}{2}\sqrt{3\lambda_2})$ **(c)** $\lambda_1 \in (-\frac{1}{2}\sqrt{3\lambda_2}, -\frac{1}{2}\sqrt{\lambda_2})$

(d) $\lambda_1 = -\frac{1}{2}\sqrt{\lambda_2}$ **(e)** $\lambda_1 \in (-\frac{1}{2}\sqrt{\lambda_2},0)$ **(f)** $\lambda_1 \in (0,\sqrt{\lambda_2})$ **(g)** $\lambda_1 > \sqrt{\lambda_2}$

Figure 3.8: Dynamics in P_2

4 The GEOFLOW-Experiments

The final chapter of this thesis is devoted to the geophysical origin of the spherical Bénard problem and the GEOFLOW-experiments. In the first section some information on the internal structure of the Earth is given and we explain the role that convective fluid movement plays regarding phenomena such as the reversals of polarity of the Earth's magnetic field. The rest of this chapter deals with the GEOFLOW-experiments, an empirical approach to the study of fluid dynamics in a spherical shell, realized in the microgravity environment of the International Space Station.

4.1 Geophysical Background

Let us first take a look at the geophysical background that provides the primary motivation for the study of the spherical Bénard problem. The information in this section is due to [Fowler (2008)], mainly Chapter 8, and represents the current state of geophysical research.

We begin by describing the major internal divisions of the Earth as depicted in Figure 4.1. On average the outer crustal layer of the Earth is 38km thick beneath continents and 7-8km beneath oceans. It is, loosely speaking, of granitoid composition, rich in silica (SiO_2) and rather thin compared to the radius of the Earth which is approximately 6300km. Beneath this crust lies the mantle which is solid and extends down about 2900km to the Earth's central core. It is mainly composed of magnesium silicates and therefore both physically and chemically distinct from the crust. The crust has emerged from the mantle over millions of years over a series of melting and reworking processes and the boundary between the two is full of geophysical activity that triggers volcanism and influences plate tectonics. Further beneath the mantle lies the core of the Earth. Its existence was first deduced by R.D. Oldham in 1906 from studies of earthquake data that showed that there must be another region deep down in the Earth that is physically and chemically different from both the mantle and the crust. The core predominantly consists of iron and was at first believed to be fluid until in 1936 a Danish seismologist, Inge Lehmann, was able to derive (again from earthquake data) that there must be a solid inner core that is surrounded by a liquid outer one.

This internal structure of the Earth features two regions where convective motion arises:

- In the mantle, where convection takes place at time scales of millions of years and is thought to have an influence on plate tectonics

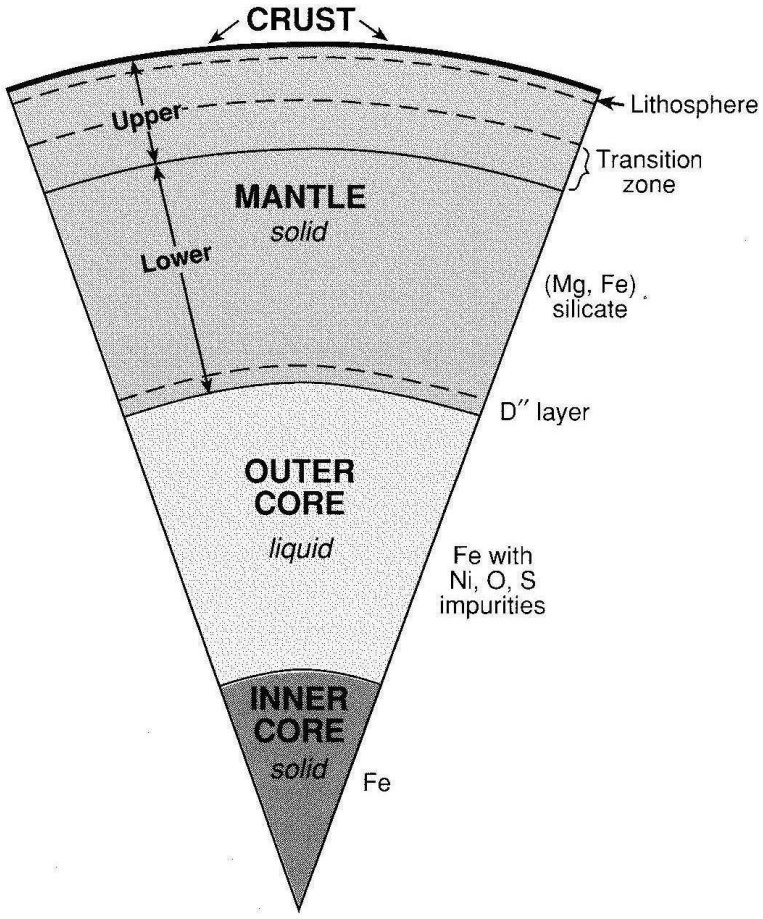

Figure 4.1: Interior of the Earth, from [Fowler (2008)]

- In the outer core, where convection seems to be related to the evolution of the Earth's magnetic field

Let us take a closer look at both of these regions to explain where and why convective motions occur.

The Mantle

Since even the deepest borehole that has ever been drilled penetrates the Earth's crust just a tiny 12km our knowledge of the chemical composition of the deeper regions of the Earth must come from elsewhere. Indeed there are sophisticated geochemical methods that use the composition of rocks that originate from the mantle and have come to the surface through volcanism to draw conclusions about the composition of the inner layers of the Earth. Moreover, experiments on the behavior of minerals that could exist in the mantle under extremely high pressure and temperature conditions staunchly support the assumption that the mantle is composed mainly of magnesian silicate in the form of olivine.

The high temperature and pressure in the mantle cause its viscosity to be low enough for viscous flow to take place, but only on a geological timescale of millions of years. Even

though the mantle is composed of solid material it is mechanically weak compared to the stronger outermost shell. If one views the Earth as a heat engine, the crust is an outer skin through which heat is lost via conduction whereas the main regions of the mantle transport heat from the core upwards by means of convection.

The fact that the mantle mainly consists of olivine leads to the conjecture that there is a boundary, approximately 670km deep, where the mantle undergoes phase changes due to chemical properties that depend on pressure. The mantle is thus divided into an upper and a lower part. Convection is caused by density differences that are due to a temperature gradient: The outer core is hotter than the lower mantle and this drives convection. It is not entirely clear, however, whether or not the upper and lower mantle convect separately. Possibly the most interesting question regarding mantle convection is whether or not it controls plate tectonics. In a sense, this is a "chicken or the egg" type of issue: Do the tectonic plates move because they are dragged around by the motions of the mantle underneath or does the mantle move because the forces at the edges of the plates drive the plates which then drag the mantle with them? It is possible to shed some light on this question by balancing the relevant driving and resistive forces against each other but there is still much that we do not know about flow in the mantle and plate tectonics.

The Core

For the core it is even more difficult to obtain information about its chemical structure since there is no way to get hold of a direct sample. Therefore one approach is to look at the elements of which the Sun and also meteorites consist since our planet is believed to have originated from the aggregation of meteoritic material. Meteorites can be divided into two main types: stony and iron. The former is similar in composition to the mantle of the Earth and there is evidence to suggest that the latter corresponds to deeper regions within our planet, the core. Following this line of reasoning the core consists mainly of iron and iron alloys. However, not much is known about the chemical processes that led to the creation of the Earth and knowledge about its chemical and thermal evolution is also based on rather vague assumptions. Still measurements of seismic velocity seem to support this theory. This and deductions about the density structure within the Earth have led scientists to believe quite strongly that iron is the main component of which the core is made. The outer core is in fact probably an iron alloy while the inner core may well consist almost purely of iron. The most favored candidates for the alloying materials are nickel, oxygen, hydrogen, silicon and carbon. More evidence can be gathered through shock wave experiments that allow for density estimates of the core. These rule out the possibility of a pure iron or nickel-iron outer core since those materials are too heavy. High-pressure and temperature experiments suggest that oxygen is very likely to be present in the core.

These uncertainties about the exact chemical composition lead to large error intervals in

temperature estimations for the core: The presence of oxygen, for example, would raise the melting temperature and because the outer core is known to be liquid this would suggest higher core temperatures. Estimates of the temperature within the core also depend on assumptions made about mantle convection, in particular whether or not the upper and lower mantle convect separately. For all these reasons the temperature at the center of the Earth cannot be determined more accurately than $6000\text{K} \pm 500\text{K}$.

The fact that the outer core is liquid and the inner core is solid is believed to be a consequence of the melting curve for iron. The temperature in the inner core lies below the melting temperature (at that particular pressure) so it is solid. In the outer core the temperature is higher than the melting temperature of iron, so it is liquid. Of course the actual melting curve also depends on the impurities and alloying materials. The temperature distribution within the core is of interest because it determines the state of the core-mantle and inner core-outer core interface and thus serves as a driving force for core convection as well as mantle convection.

Let us now explain briefly the role that core convection plays for the Earth's magnetic field. The dominant field is a dipole and paleomagnetic evidence exists to suggest that it has been present for at least 3.5 billion years. It has been known since around 1600 that the origin of the magnetic field, e.g. magnetized material or an electrical current system creating a dynamo effect, must be located inside the Earth itself. There are four possible explanations for the existence of such a field:

- a magnetic dipole at the center of the Earth
- a uniformly magnetized Earth
- a uniformly magnetized core
- an east-west electrical current flowing around the core-mantle boundary

The chemical composition of the mantle (silicates) rules out the possibility of mantle dynamics producing the magnetic field. Temperature estimates (even though highly inaccurate) for the core eliminate the second and third possibility because the temperature definitely exceeds the Curie points for magnetic minerals, i.e., the temperatures above which no permanent magnetization is possible (see section 3.1.3 in [Fowler (2008)] for more details).

Moreover, the magnetic field is not stationary in time as current measurements show that its strength is slightly decreasing and the poles are slowly drifting. It even undergoes irregular reversals of polarity and this also makes it unlikely that the core is uniformly magnetized or that there exists a dipole at the center.

The best explanation that there currently is for the presence of such a magnetic field offers the theory of geodynamos. An electrical current system within the core is believed to act as a

dynamo keeping up the magnetic field while changes in the flow patterns account for its non-stationary nature. Even simple mechanical models of self-exciting dynamos can reproduce the behavior of the Earth's magnetic field in the sense that they exhibit irregular reversals of polarity, see for example Chapter 7.4 in [Ghil and Childress (1987)]. The system of nonlinear partial differential equations that describes the full magnetohydrodynamic problem is complicated and exceedingly difficult to tackle. That is why several, qualitatively different approaches to obtain a partial solution are pursued:

- start with a velocity field for the core and determine the magnetic field it generates
- determine what kind of velocity field could be present in the core at all, without taking into account magnetic activity

One further important aspect that needs to be considered is the question what drives the geodynamo, i.e., what drives convection in the core of the Earth. Convection is always due to a density gradient which in turn can result from different sources such as a temperature gradient, changes in the rotation of the Earth or differences in the chemical composition of the core. A convenient explanation for core convection would be the so called primordial heat, the heat resulting from the formation of the Earth, which the core is slowly giving up. This would imply that the inner core is cooling, therefore solidifying and growing while consuming the liquid outer core. Still it is also likely that chemical aspects cause the density differences. It is a question that has not been answered exhaustively to date.

Aperiodic reversals of polarity

To finish this section we give a brief overview of what is known about the reversals of polarity that the magnetic field exhibits. They occur at irregular intervals of at least tens of thousands of years and can be detected by the magnetization of volcanic rocks or iron oxide grains in sedimentary layers. By determining the age of those rocks or layers it is then possible to identify periods of time during which the magnetic poles must have been in a position approximately opposite to where they are today. When the poles are about to swap positions the field decreases to around 10% of its usual strength and undergoes oscillations of increasing angle until the actual reversal occurs. Then the field strength increases and the positions of the poles become more stable again. This process takes place in a geologically short period of time of 5000 years or less.

This intermittent behavior where the system (the magnetic field) spends a long time in the neighborhood of an equilibrium (one state of polarity) and then all of a sudden rapidly moves close to some distant other equilibrium is called **stop-and-go dynamics**. It is reminiscent of a trajectory near a heteroclinic cycle as explained in section 3.5. This leads us to the conjecture that heteroclinic cycles in the flow structures of the Earth's core are responsible for the aperiodic reversals of the magnetic field.

4.2 Experimental Set-up

The *Chair of Aerodynamics and Fluid Mechanics* at the Technical University of Brandenburg (BTU) in Cottbus, Germany, conducted a series of experiments in the Fluid Science Laboratory (FSL) of the International Space Station (ISS) in 2008/2009. The project is called GEOFLOW, which is short for "geophysical flow simulation". Its purpose is the investigation of pattern formation and stability in the setting of the spherical Bénard problem and thus to empirically verify theoretical and numerical results in order to gain a deeper understanding of the geophysical phenomena described in the previous section. In this section we give an overview of the experimental set-up, cf. [Egbers et al. (2003)] as a reference.

A major difficulty in conducting such experiments is that a microgravity environment is needed to get rid of the unidirectional gravitation that is always present under terrestrial conditions. In general three methods are known to provide such an environment:

- Flying far out into space where all celestial bodies are far enough away for gravity to be neglected
- free fall, e.g. in drop towers or parabolic flights
- orbiting a planet

The first possibility may be the simplest in conception but is not feasible due to extreme technical difficulty and costs. Free fall can only be realized for a rather short period of time, e.g. parabolic flights provide weightlessness for a maximum of 20 seconds. For experiments with a great variety of parameter sets microgravity times of days and weeks are required. This is the unique feature that distinguishes the GEOFLOW-experiments from those conducted before, such as the space shuttle experiments that [BTU Cottbus (2008)] mentions on page 8. Microgravity is achieved through orbiting a planet, which actually means perpertual free fall, i.e., falling with sufficient tangential speed so as to follow the curvature of the planet (the Earth). This is the environment that is experienced on the ISS and it offers suitable conditions for an unbiased experimental setting for the Bénard problem.

The Fluid Science Laboratory is a part of Columbus, a science laboratory on the ISS that is run by the European Space Agency. It supports scientific microgravity research in fluid dynamics by making it possible to observe phenomena inside of transparent and at the surface of opaque fluids. Direct viewing of the experimental volume with different cameras is only one of various possibilities to do so: Velocimetry techniques such as electronic speckle pattern interferometry and the Schlieren method can be used to visualize flow structures. We do not go into too much detail on the technical aspects of the experiments here, a complete list of what the laboratory offers can be found in [Egbers et al. (2003)].

Table 4.1: Parameters

Parameter	GEOFLOW I	Earth (mantle)	Earth (core)
Rayleigh number (C_ℓ or Ra)	$\leq 1.4 \cdot 10^5$	$10^6 - 10^8$	$> 10^{25}$
Prandtl number ($\mathcal{P}$)	64.64	temp. dependent	$0.1 - 1.0$
Radius ratio (η)	0.5	0.55	0.35
Taylor number (Ta)	$\leq 1.3 \cdot 10^7$	$\ll 1$	$\approx 10^{28}$

To imitate the gravity field acting on a planet a central, radially symmetric force field is imposed on the domain by applying a high voltage potential difference to the inner and outer sphere and exploiting the resulting dielectrophoretic effect. This is where we encounter a first difference between the experiments and reality: The dielectrophoretic force field is an r^{-5} field whereas gravitation in the interior of the Earth increases linearly with the radius. The latter follows from Newton's law of universal gravitation which states that for spherically symmetric masses gravitation acts as if the entire mass was concentrated at one point in the center. If we combine this with the fact that outside the sphere gravity is an r^{-2} field and assume constant density ρ we can calculate the gravitational force at a point x at radius r inside the Earth as

$$M \cdot \frac{G}{r^2} = \frac{4}{3}\pi r^3 \rho \cdot \frac{G}{r^2} = \frac{4}{3}\pi \rho G r$$

where M is the mass inside of r and G is the gravitational constant. Despite this inaccuracy of the experimental set-up there is evidence to suggest that the characteristic flow patterns remain the same so that it is still reasonable to expect geophysically relevant results, cf. [BTU Cottbus (2008)]. Another specificity worth mentioning is the fact that a thin conductor wire inside the shell is necessary to control the potential difference between the spheres. This breaks the $O(3)$-symmetry of the experiment and could have significant influence on the resulting flow structures.

The GEOFLOW Experiment Container (EC) has been designed to implement the aforementioned technique of generating a force field and conduct the experiments. Due to the high modularity of the FSL the EC requires no crew time except for the initial integration into the laboratory and locking and unlocking for running the experiments. For an extensive description of its properties see [Egbers et al. (2003)], we just state the technical facts that are interesting from our point of view. The radius ratio η was chosen as 0.5, a medium gap width approximately corresponding to the order of magnitude found inside the Earth. Of course the inner sphere can be heated and the outer one cooled as the temperature gradient is the primary quantity to be varied. It is also possible to rotate both spheres and thus to observe the influence of the Taylor/Reynolds number. A list of the parameters and the range in which they can be adjusted compared to the values for mantle and core convection is given in Table 4.1. Note that both the Taylor (Ta) and the Reynolds number (Re) are dimensionless quantities that characterize the importance of inertial (centrifugal) forces relative to viscous

forces and thus measure the rate of rotation. In the context of the spherical Bénard problem different authors use either of them. In fact, the square root of the Taylor number is a rotating Reynolds number and therefore when $Ta = 0$ we always have $Re = 0$ and vice versa.

GEOFLOW I - Convection in the outer core

The GEOFLOW EC was brought to the ISS in February 2008 in the course of NASA Space Shuttle Mission STS-122. Experiments were scheduled to be conducted in 36 runs, starting in August 2008 and completed by January 2009. Due to interruptions and delays caused by traffic on orbit, other experiments, etc. only one third of the runs was completed. Silicone oils with different viscosities were used as working fluid so that the influence of the Prandtl number $\mathcal{P}$ could be observed. Since the viscosity of these oils is as good as independent of temperature these experiments resembled the situation in the outer core of the Earth rather than in the mantle. Downloading of image data (interferograms) was controlled by the Italian Microgravity and Advanced Research Center. The images were received with a time delay of one day and distributed to the cooperating research centers across Europe. Around $100{,}000$ images have been collected from GEOFLOW I, amounting to 100GB of data that must now be evaluated with regard to the classification of flow structures.

GEOFLOW II - Convection in the Mantle

The results of the experiments and their successful first interpretation call for a rerun to examine more situations in detail. A second GEOFLOW mission is scheduled for the fall of 2010. This time the focus lies on the modeling of convection in the mantle of the Earth. In contrast to the outer core of the Earth here the viscosity of the fluid is highly dependent on its temperature. Therefore in GEOFLOW II the working fluid will be an alkanol with temperature-dependent viscosity, such as nonanol ($C_9H_{20}O$) or octanol ($C_8H_{18}O$). The conduction and documentation of the experiments will be similar to GEOFLOW I and can be realized with the same technical equipment. Different flow patterns and new insights can definitely be expected.

4.3 Numerical Results

In this section we briefly summarize the numerical efforts that have been made prior to the conduction of the GEOFLOW I experiments in order to assist in the design of the experiments, e.g. by determining parameter values that can be expected to exhibit particularly interesting dynamics. Additional information on what we display in this section can be found in [Travnikov et al. (2003)].

The case where $\mathrm{Ta} = 0$, no rotation

According to [Travnikov et al. (2003)] another suitable reparametrization transforms the perturbation equations (3.1), (3.4) and (3.5) into

$$\begin{cases} \mathcal{P}^{-1}\dfrac{\partial u}{\partial t} & = -\nabla p + \Delta u + \dfrac{\eta^2}{(1-\eta)^2} Ra \dfrac{\theta}{r^5} x \\ \dfrac{\partial \theta}{\partial t} & = -\langle u, \nabla T \rangle + \Delta\theta \\ \text{div } u & = 0 \end{cases} . \tag{4.1}$$

Note that now in the context of the GEOFLOW-experiments we denote the Rayleigh number by Ra instead of C_ℓ, in accordance with [Travnikov et al. (2003)]. Their definition differs slightly from that of [Chandrasekhar (1961)] which we introduced in section 3.3, but that is of no significance since the definitions are equivalent in the sense that both numbers are proportional to the temperature gradient. From system (4.1) we can immediately conclude that the Prandtl number $\mathcal{P}$ does not influence the critical Rayleigh number Ra_{crit} if $\frac{\partial u}{\partial t} = 0$ which is the case when the bifurcation is steady-state. As we have seen in section 3.1 this can be shown to be true, at least under certain additional assumptions. So we might expect the numerical results to reflect this, and indeed they do: As [Travnikov et al. (2003)] determined for calculations with radius ratios from 0.1 to 0.9 with steps of 0.02 and Prandtl numbers $1, 10, 100$ the bifurcation turned out to be steady-state and Ra_{crit} depends on η only. Note that the force term in the equations differs from what [Chandrasekhar (1961)] determined because now we consider a dielectrophoretic force field rather than the gravitational field.

Another theoretical prediction, namely Proposition 36, is confirmed by the fact that for η tending to 1 the index of the most unstable mode tends to infinity as can be seen in Figure 4.2. We also see that for $\eta > 0.6$ it becomes more and more difficult to distinguish the different modes. A very small interior shell is harder to implement technically which is why $\eta = 0.5$ was chosen for the experiments. Then the first unstable mode should be $\ell = 4$. From Figure 4.2 it is also clear that the 1-2 mode interaction for which we analyzed the existence of heteroclinic cycles in section 3.5 cannot be reached in the experiments since it occurs for η significantly smaller than 0.5. Further calculations showed that for $\eta \approx 0.4466$ the 3-4 mode interaction is expected, as stated in [Gellert et al. (2005)]. In a (possibly very small) neighborhood of this parameter value heteroclinic cycles exist that are more complex than those we investigated for the 1-2 interaction. However, even though this radius ratio is not too far away from 0.5 this interaction is difficult to examine empirically because of the sensitive dependence on η.

The case where $\mathrm{Ta} \neq 0$, rotation

In this case the perturbation equations look slightly different (see [Travnikov et al. (2003)]) and the critical Rayleigh number does depend on the Prandtl number $\mathcal{P}$. However, the solutions exhibit very similar behavior for all $\mathcal{P}$. For very fast rotation speeds, i.e., large Taylor

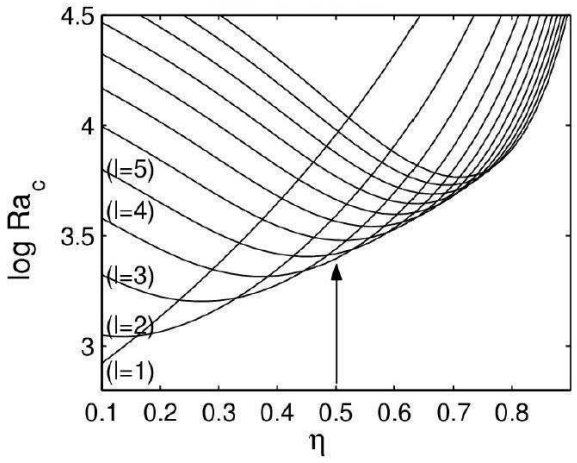

Figure 4.2: Unstable Modes, from [BTU Cottbus (2008)]

numbers Ta, the results for the critical Rayleigh number for the onset of convection tend to $Ra_{crit} \sim Ta^{2/3}$. The computational requirements are much larger than in the non-rotating case. Since we focused on that case in our theoretical analysis we do the same here and this should suffice as an indication of the numerical results for rotating shells. For more details such as actually calculated stability curves in dependence of the Taylor number Ta see [Travnikov et al. (2003)].

4.4 Experimental Results

In this final section we want to give a first impression of the experimental results that have been obtained so far and explain how the experimental data is evaluated. As a reference for this information see [Futterer et al. (2010)].

The most important method to obtain images of the flow structures is the Wollaston shearing interferometry. It is an enhancement of classical interferometry where light waves are sent through the medium and their interference pattern is studied. When two waves of the same frequency meet their phase difference determines the resulting interference pattern: Waves that are in phase will undergo constructive interference, i.e., increasing the amplitude, while waves that are out of phase undergo destructive interference where the amplitude decreases. Typically a beam of light is split into two identical beams that then travel through the medium along different paths until they are recombined. The phase difference at the point of recombination is then diagnostic of any differences along the two paths the beams have taken. In particular, changes in the refractive index of the medium can be detected in this way. Since the refractive index is sensitive to a density gradient and thus to a temperature gradient this is an effective way of making convection visible.

In the resulting images, the interferograms, convective motion corresponds to fine fringes

as can be seen in Figure 4.4. The pictures show a slanted view of the spheres from above, such that the north pole is in the upper region of the picture. For the runs where the shell is rotating the camera took a photo every 60°. In order to classify the observed flow patterns and identify sub- and supercritical regimes the fringe structures in the images are examined. A comparison of Figures 4.3 and 4.4 shows that for lower Rayleigh numbers there are no fringes which means we see a purely conductive state. The occurrence of the first fringes corresponds to the onset of convection. With increasing Rayleigh and/or Taylor number more and more regions of the sphere, starting with the north pole area, are covered by fringes because they display fluid motion that causes a change in the refractive index of the fluid which leads to a relevant phase change of the passing light beams.

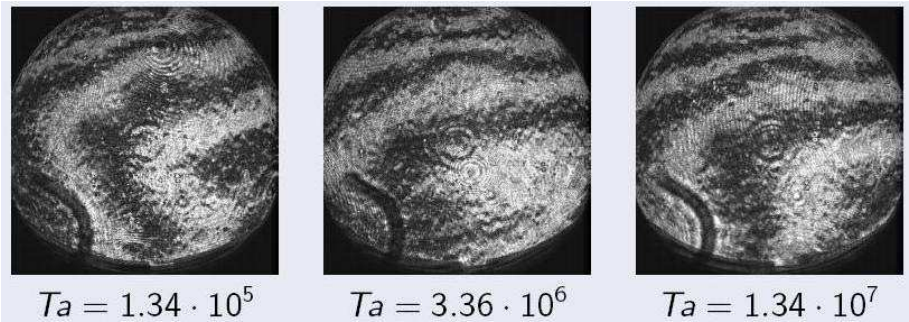

Figure 4.3: Interferograms for $Ra = 4 \cdot 10^3$, from [Koch et al. (2008)]

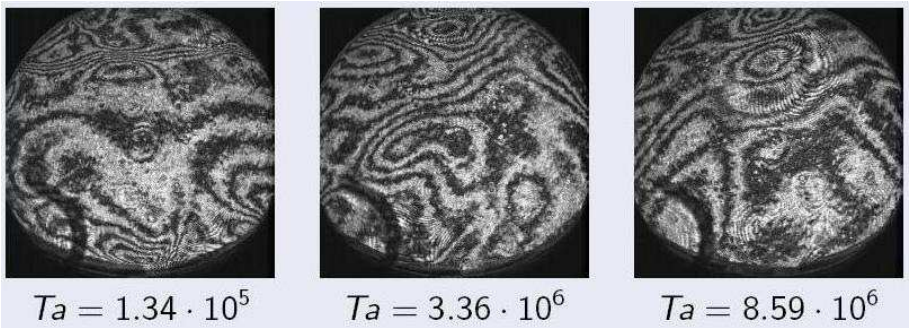

Figure 4.4: Interferograms for $Ra = 8.87 \cdot 10^4$, from [Koch et al. (2008)]

To get a more reliable impression of which interferogram corresponds to which flow pattern artificial interferograms are created from the numerically calculated results. The two interferograms are then compared which allows for a more detailed evaluation of the experimental interferograms. This process of data analysis is schematically depicted in Figure 4.5. In comparison to the numerical results there seems to be a slight shift in the stability line to higher values for the critical Rayleigh numbers as [Futterer et al. (2010)] observe. This is probably due to the fact that while the numerical calculations can be performed with an error of just 1% it is technically difficult yet crucial for the experiments to maintain the relevant parameter values at the desired level over the course of a run. Especially the maintenance of the temperature gradient causes errors of up to 10%.

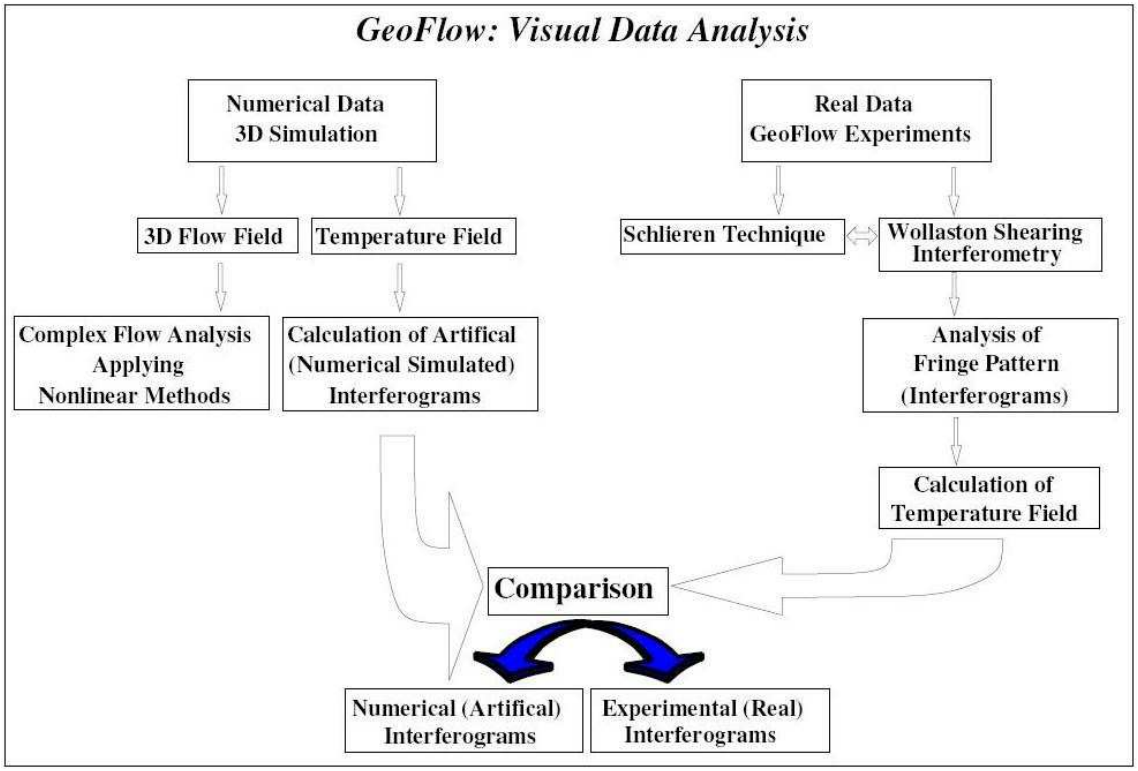

Figure 4.5: Data Analysis for GEOFLOW, from [BTU Cottbus (2008)]

The analysis of the abundance of image data has not yet been completed. More interesting results on the classification of supercritical flow structures can be expected. A more detailed investigation will show if the presence of heteroclinic cycles can also be verified experimentally. And of course new data from GEOFLOW II will soon help to shed more light on phenomena of mantle convection.

5 Summary

Here we shortly review the goal and the results of this thesis and outline several further research ideas that went beyond the scope of this work.

We performed a mathematical bifurcation analysis of the spherical Bénard problem for an incompressible fluid in a spherical gap where the inner boundary is heated and a radially symmetric gravity field is present. In particular, the onset of convection was studied in dependence of the Rayleigh number. The corresponding bifurcation turned out to be steady-state under certain assumptions which was confirmed by numerical results for the GEOFLOW-experiments. We also proved that the index ℓ of the most unstable mode tends to infinity if the gap width becomes arbitrarily small. This led to the discovery of mode interaction cases – parameter values for which two eigenspaces V_ℓ and $V_{\ell+1}$ lose their stability at the same time. We investigated the 1-2 mode interaction more closely: The center manifold theorem allowed us to project the infinite-dimensional system onto the space $V = V_1 \oplus V_2$ where $\dim(V) = 8$. We then investigated the isotropy lattice and made use of the $O(3)$-symmetry of the differential equations, the equivariant branching lemma guaranteed the existence of solutions with the symmetries of maximal isotropy subgroups. For the 1-2 mode interaction case we were then able to derive the existence of heteroclinic cycles.
Finally we elaborated on the geophysical background of the Bénard problem, particularly mantle and core convection inside the Earth. We also discussed the aperiodic reversals of the Earth's magnetic field and possible relations to heteroclinic orbits in the flow patterns of the outer core. Furthermore, we analyzed the results of the GEOFLOW-experiments, explained how they were conducted and gave an idea of the data evaluation process.

The geophysical background of this field of research immediately suggests several variations to the problem we treated. An obvious next step would be to break the $O(3)$-symmetry of the equations by letting the domain rotate around an axis, just like the Earth does. This perturbation reduces the symmetry to $SO(2) \times \mathbb{Z}_2^c$ and has been investigated by several authors, for example [Chossat (1979)]. From a physical point of view the loss of symmetry in this case is due to the Coriolis force.
Another relevant aspect that we have not discussed in detail is of course the Earth's magnetic dipole field. Assuming that the fluid in the shell is electrically conducting the consequent interaction of the velocity field and the magnetic field brings up more interesting research questions in the theory of geodynamos. As an example consider the question what types of velocity fields favor magnetic activity in the sense that an arbitrarily small magnetic seed

field is always amplified by the motion of the fluid to form a stable large scale magnetic field. Even though we did mention parallels between the temporal evolution of the magnetic field and heteroclinic cycles in the flow structures, note that this is a purely qualitative resemblance and we have completely excluded magnetism, i.e., Maxwell's equations, from our investigation.

Many questions like these are far from being answered exhaustively and the author of this thesis would very much like to engage in further research dedicated to shedding more light on these topics in the future.

Bibliography

Armbruster, D. and Chossat, P. (1991). Heteroclinic orbits in a spherically invariant system. *Physica D*, 50: pages 155–176.

Backus, G. (1986). Poloidal and Toroidal Fields in Geomagnetic Field Modeling. *Reviews of Geophysics*, 24: pages 75–109.

Beltrame, P., Egbers, C., and Hollerbach, R. (2003). The Geoflow-Experiment on ISS (Part III): Bifurcation Analysis. *Adv. Space Res.*, 32: pages 191–197.

BTU Cottbus (2008). Abschlussbericht: Auslegung und Betrieb eines Laborbreadboards für die Integration des Kugelspaltexperiments in den FSL-Experiment-Container. (Lehrstuhl für Aerodynamik und Strömungslehre).

Chandrasekhar, S. (1961). *Hydrodynamic and Hydromagnetic Stability*. Oxford University Press.

Childress, S. and Gilbert, A. (1995). *Stretch, Twist, Fold: The Fast Dynamo*. Springer Verlag Berlin.

Chossat, P. (1979). Bifurcation and Stability of convective flows in a rotating or not rotating spherical shell. *SIAM J. Appl. Math.*, 37: pages 624–647.

Chossat, P., Guyard, F., and Lauterbach, R. (1999). Generalized Heteroclinic Cycles in Spherically Invariant Systems and Their Perturbations. *J. Nonlinear Sci.*, 9: pages 479–524.

Doedel, E. and Oldeman, B. (2009). AUTO-07P: Continuation and Bifurcation Software for Ordinary Differential Equations. (Concordia University Montreal, Canada).

Duff, G. and Naylor, D. (1966). *Differential Equations of Applied Mathematics*. John Wiley & Sons New York.

Egbers, C., Beyer, W., Bonhage, A., Hollerbach, R., and Beltrame, P. (2003). The Geoflow-Experiment on ISS (Part I): Experimental Preparation and Design of laboratory testing hardware. *Adv. Space Res.*, 32: pages 171–180.

Fowler, C. (2008). *The Solid Earth*. Cambridge University Press, fourth edition.

Friedrich, R. and Haken, H. (1986). Static, wavelike and chaotic thermal convection in spherical geometries. *Physical Rev. A*, 34: pages 2100–2120.

Futterer, B., Egbers, C., Dahley, N., Koch, S., and Jehring, L. (2010). First identification of sub- and supercritical convection patterns from "GeoFlow", the geophysical flow simulation experiment integrated in Fluid Science Laboratory. *Acta Astronautica*, 66: pages 193–200.

Gellert, M., Beltrame, P., and Egbers, C. (2005). The GeoFlow experiment - spherical Rayleigh-Bénard convection under the influence of an artificial central force field. *Journal of Physics: Conference Series*, 14: pages 157–161.

Ghil, M. and Childress, S. (1987). *Topics in Geophysical Fluid Dynamics: Atmospheric Dynamics, Dynamo Theory, and Climate Dynamics*. Springer Verlag New York.

Golubitsky, M. and Schaeffer, D. G. (1985). *Singularities and Groups in Bifurcation Theory*, volume 1. Springer Verlag New York.

Golubitsky, M. and Stewart, I. (2002). *The Symmetry Perspective*. Birkhäuser Verlag.

Golubitsky, M., Stewart, I., and Schaeffer, D. G. (1988). *Singularities and Groups in Bifurcation Theory*, volume 2. Springer Verlag New York.

Henry, D. (1981). *Geometric Theory of Semilinear Parabolic Equations*. Springer Verlag Berlin.

Joseph, D. D. (1976). *Stability of Fluid Motions I*. Springer Verlag Berlin.

Koch, S., Dahley, N., Futterer, B., and Egbers, C. (2008). Das GeoFlow-Experiment auf der ISS: Auswertung erster Experimentdaten. (Fachtagung "Lasermethoden in der Strömungsmechanik" Karlsruhe).

Kuznetsov, Y. A. (1995). *Elements of Applied Bifurcation Theory*. Springer Verlag New York.

Melbourne, I., Chossat, P., and Golubitsky, M. (1989). Heteroclinic cycles involving periodic solutions in mode interactions with $O(2)$-symmetry. *Proc. Royal Soc. Edinburgh*, 113A: pages 315–345.

Palis, J. and de Melo, W. (1982). *Geometric Theory of Dynamical Systems*. Springer Verlag New York.

Travnikov, V., Egbers, C., and Hollerbach, R. (2003). The Geoflow-Experiment on ISS (Part II): Numerical Simulation. *Adv. Space Res.*, 32: pages 181–189.

I, Alexander Lohse, assure that this diploma thesis was prepared by myself with the common help provided by my supervisors using no other than the denoted sources.

Hamburg, July 2010